

Impact of Solar Geoengineering on Wildfires in the 21st Century in CESM2/WACCM6

Wenfu Tang¹, Simone Tilmes¹, David M. Lawrence², Fang Li³, Cenlin He⁴, Louisa K. Emmons¹, Rebecca R. Buchholz¹, Lili Xia⁵

¹Atmospheric Chemistry Observations & Modeling Laboratory, National Center for Atmospheric Research, Boulder, CO, USA

²Climate and Global Dynamics Laboratory, National Center for Atmospheric Research, Boulder, CO, USA

³International Center for Climate and Environment Sciences, Institute of Atmospheric Physics, Chinese Academy of Sciences, Beijing, China

⁴Research Applications Laboratory, National Center for Atmospheric Research, Boulder, CO, USA

⁵Department of Environmental Sciences, Rutgers University, New Brunswick, NJ, USA

Correspondence: Wenfu Tang (wenfut@ucar.edu)

Abstract

We quantify future changes of wildfire burned area and carbon emissions in the 21st century under four Shared Socioeconomic Pathways (SSPs) scenarios and two SSP5-8.5-based solar geoengineering scenarios with a target surface temperature defined by SSP2-4.5: solar irradiance reduction (G6solar) and stratospheric sulfate aerosol injections (G6sulfur), and explore the mechanisms that drive solar geoengineering impacts on fires. This study is based on fully coupled climate-chemistry simulations with simulated occurrence of fires (area burnt and carbon emissions) using the Whole Atmosphere Community Climate Model Version 6 (WACCM6) as the atmospheric component of the Community Earth System Model Version 2 (CESM2). Globally, total wildfire burned area is projected to increase over the 21st century under scenarios without geoengineering and decrease under the two geoengineering scenarios. By the end of the century, the two geoengineering scenarios have lower burned area and fire carbon emissions than not only their base-climate scenario SSP5-8.5 but also the targeted-climate scenario SSP2-4.5.

Geoengineering reduces wildfire occurrence through decreasing surface temperature and wind speed and increasing relative humidity and soil water, with the exception of boreal regions where geoengineering increases the occurrence of wildfires due to a decrease in relative humidity and soil water compared to present day. This leads to a global reduction in burned area and fire carbon emissions by the end of the century *relative to* their base-climate scenario *SSP5-8.5*. However, geoengineering also yields reductions in precipitation compared to a warming climate, which offsets some of the fire reduction. Overall, the impacts of the different driving factors are larger on burned area than fire carbon emissions. In general, the stratospheric sulfate aerosol approach has a stronger fire-reducing effect than the solar irradiance reduction approach.

44 **1. Introduction**

45 Fire is an important component of the Earth system. It directly impacts climate in two main
46 ways. First, the burning of biomass is one of the major sources of radiatively and/or chemically
47 active trace gases and aerosols in the atmosphere (Andreae and Merlet, 2001; Li et al. 2022).
48 Second, fires pose alterations to terrestrial ecosystem states and functioning such as changing
49 vegetation distribution and structure, disturbing the carbon cycle and water cycle, and changing
50 surface albedo (Bowman et al., 2009; Li and Lawrence, 2017; Liu et al., 2019; Lasslop et al. 2020).
51 In addition to the impact on climate, fires also have significant impacts on air quality and weather
52 across spatial scales (e.g., Bowman et al., 2009, Tang et al., 2022). For example, fires degrade air
53 quality and human health as many of the emitted gases and aerosols from fires are primary
54 pollutants or precursors to secondary chemically-produced pollutants (Wiedinmyer et al., 2006;
55 van der Werf et al., 2006). Fires also alter regional dynamics and weather through changing surface
56 heat and water vapor fluxes, convection, clouds, and precipitation (e.g., Bowman et al., 2009; Coen
57 et al., 2013, Zhang et al., 2022).

58 Fire is regulated by various factors, including weather and climate conditions (e.g., soil
59 moisture, temperature, precipitation, and wind speed), vegetation composition and structure, and
60 human activities (e.g., land use and land cover change, human ignition and suppression) (e.g., Li
61 et al., 2013; Chen et al., 2017; Knorr et al., 2016a, 2016b; Li et al., 2018; Pechony and Shindell,
62 2010; van der Werf et al., 2008). These factors also interact with each other in the Earth system
63 (e.g., Walker et al., 2020; Loehman, 2020). For example, climate can alter vegetation composition
64 and structure, and vegetation can also impact climate and weather through evapotranspiration. Due
65 to the complex interactions and feedbacks among these factors and fires, quantifying and
66 projecting the trend of fires is challenging and is subject to large uncertainties. Despite challenges
67 and uncertainties, previous studies have generally suggested that in the future global fire risk will
68 increase, though with significant regional differences (e.g., Abatzoglou et al., 2019; Bowman et
69 al., 2020; Di Virgilio et al., 2019; Flannigan et al., 2009, 2013; Ford et al., 2018; Huang et al.,
70 2015; Li et al., 2020; Liu et al. 2010; Luo et al., 2013; Pechony and Shindell, 2010; Veira et al.,
71 2016). The growing importance combined with large uncertainties of fires has posed an urge to
72 understand and quantify future fire trends in the context of climate change. It has been suggested
73 that future climate mitigation should consider the impact of fires (Shiogama et al., 2020; Ward et
74 al., 2012).

75 The Shared Socioeconomic Pathways (SSPs) were established to facilitate the integrated
76 analysis of future climate impacts, vulnerabilities, adaptation, and mitigation (Riahi et al., 2017).
77 These SSP scenarios utilized in Phase 6 of the Coupled Model Intercomparison Project (CMIP6)
78 were generated with integrated assessment models, based on five narratives describing alternative
79 socio-economic developments, including sustainable development (SSP1), middle-of-the-road
80 development (SSP2), regional rivalry (SSP3), inequality (SSP4), and fossil-fueled development
81 (SSP5). Different scenarios have different energy, land use, and emissions implications.
82 Corresponding global population projections consistent with each of the SSPs have also been
83 established (Jones and O'Neill, 2016).

84 Solar geoengineering, also known as solar radiation modification (SRM) or more generally as
85 climate intervention, has been researched as a potential option to offset some of the radiative
86 effects of increasing anthropogenic greenhouse gases in the future through solar radiation

87 modification (e.g., Kravitz et al., 2015; Tilmes et al., 2009, 2020). One proposed approach is to
88 inject the precursor of sulfate aerosols (sulfur dioxide; SO₂) to the stratosphere that can reflect
89 incoming solar radiation. To understand the impacts of sulfate aerosols compared to direct solar
90 irradiance reduction, both experiments have been performed in parallel (e.g., Xia et al, 2016,
91 Vioni et al., 2021a). Previous studies have analyzed the impact of geoengineering on climate
92 outcomes (e.g., Tilmes et al., 2013, 2020; Vioni et al., 2021a). While global surface temperature
93 targets could be reached, SRM approaches tend to overcompensate the hydrological cycle, with
94 potential consequences to other impacts on climate and the Earth system (e.g., Bala et al., 2008;
95 Tilmes et al., 2013; Lee et al., 2020). Since fire is a key component of the Earth system and the
96 drivers of fires are directly or indirectly changed by solar geoengineering, the impacts of solar
97 geoengineering on fires should also be considered when designing and assessing solar
98 geoengineering approaches.

99 In this paper, we use a fully coupled Earth system model CESM2 with WACCM6 as the
100 atmospheric component. CESM2 (WACCM6) is coupled to the Community Land Model (CLM)
101 that includes a prognostic fire scheme, which interacts with various land and atmospheric
102 processes. WACCM6 is currently not using biomass burning emissions derived from the land
103 model. A coupling of fire emissions to the atmosphere would allow to identify additional climate
104 feedback including changes to climate and the vegetation. However, while this feedback is missing,
105 the fire model still responds to changes in the land and atmosphere and is therefore suited to
106 investigate how fires change in the 21st century. We analyze the future trends of burned area and
107 fire carbon emissions under the two geoengineering scenarios and SSP scenarios, and then analyze
108 how the two solar geoengineering approaches impact fire activity. This paper is organized as
109 follows: Section 2 describes the model simulations; Section 3 presents the future trends of burned
110 area and fire carbon emissions under SSP scenarios and geoengineering scenarios. Section 4
111 discusses how geoengineering impacts fire, and Section 5 concludes the study.

112

113 **2. Model descriptions and simulations**

114 **2.1 CESM2 (WACCM6)**

115 CESM2 (WACCM6) is a community model that has components of ocean, atmosphere, land,
116 sea-ice, land-ice, river, and wave models. These components are coupled in CESM2 by exchanging
117 states and fluxes via a coupler (Danabasoglu et al., 2019). The Community Land Model Version
118 5 (CLM5) is the land component of CESM2 (Lawrence et al., 2019). CLM uses prescribed
119 temporal land use and land cover change (LULCC), which consists of an annual time series of the
120 spatial distribution of the naturally vegetated and cropland units of each grid cell, combined with
121 the distribution of plant functional types (PFTs) and crop functional types (CFTs) existing in those
122 land units (Lawrence et al., 2019). The interactive fire scheme in the CLM5 is a key component of
123 this study and is described in more detail in Section 2.2. WACCM6 is a high-top atmospheric
124 model with 70 vertical levels and model top at ~140 km, therefore it has reasonable representation
125 of the stratosphere. The default horizontal resolution of WACCM6 is 1.25° × 0.9° (longitude ×
126 latitude). WACCM6 also includes comprehensive chemistry and aerosol mechanisms (Gettelman
127 et al., 2019; Emmons et al., 2020, Tilmes et al., 2019).

128 2.2 Description and evaluation of fire scheme in CESM2/CLM5

129 The fire scheme in CESM2/CLM5 accounts for four types of fires: agricultural fires in
130 cropland, deforestation fires in the tropical closed forests, peat fires, and non-peat fires outside
131 cropland and tropical closed forests (Li et al., 2012, 2013). Agricultural fire is accounted for in
132 these simulations but is not included in the analysis, since we focus on wildfires here. In the fire
133 scheme, burned area is affected by climate and weather conditions, vegetation composition and
134 structure, and human activities. Climate and weather conditions (e.g., temperature, precipitation,
135 wind, humidity, and soil moisture) impact natural and human ignition and fire spread through fuel
136 availability and fuel combustibility. Human activities impact deforestation fires via deforestation
137 rates that are applied from the Land Use Harmonization dataset (LUH2, Hurtt et al., 2020) that is
138 used in these experiments. Human impacts on non-deforestation and non-peat fires include both
139 ignition and suppression and are parameterized as functions of both population density and Gross
140 Domestic Product (GDP). In our setup, the global population scenarios corresponding to SSP
141 scenarios (Jones and O'Neill, 2016) are used while regionally-explicit GDP was held constant for
142 all WACCM6 simulations analyzed in this study. Fire-induced changes (including biomass and
143 peat burning, vegetation mortality, adjustment of the carbon and nitrogen (C/N) pools, carbon
144 emissions, changes in vegetation structure and functioning as well as surface water and energy
145 fluxes) are then simulated based on the calculated burned area (Li et al., 2012, 2013). These fire-
146 induced surface property changes in the land model further alter atmospheric states (i.e.,
147 temperature and water vapor) in the coupled model. Although the burned area and fire carbon
148 emissions are simulated in CLM5, our CESM2/(WACCM6) simulations use prescribed fire
149 emissions based on the CMIP6 projected inventories for trace gases and aerosols (Riahi et al., 2017)
150 for different SSPs and geoengineering scenarios. Changes in fires can have an impact on radiation,
151 precipitation, and therefore vegetation. However, since this paper mainly focuses on the impacts
152 of solar geoengineering on wildfires instead of the other way around, we do not expect the
153 uncoupled fire emissions to have a large impact on our results, but future studies will be needed to
154 further understand the impact. Full coupling of simulated fire aerosol emissions is an area of
155 ongoing development and analysis with the CESM project.

156 The fire scheme in CESM has been validated and evaluated in both uncoupled and coupled
157 versions (Li et al., 2012, 2013, 2017, 2018; Li and Lawrence 2017) and compared with other fire
158 models within the Fire Modeling Intercomparison Project (FireMIP) (Li et al., 2019). Evaluation
159 results have shown that the fire scheme can reasonably reproduce the observed amount, spatial
160 pattern, seasonality, and interannual variability of global fires, and fire-population relationship
161 under present-day climate, and has a similar historical long-term trend to the multi-source merged
162 historical reconstructions used as input data for CMIP6 (Li et al. 2018, Li et al. 2019). Although
163 the model underestimates the climate impacts on fires in boreal North America, it still performs
164 better than many other fire models (Yue et al., 2016). Here we briefly evaluate the fire carbon
165 emissions from the CESM2 (WACCM6) simulations with two satellite-based fire emission
166 inventories, namely FINNv2.5 (Fire INventory from NCAR Version 2.5; Wiedinmyer et al., 2022)
167 and GFED4.1s (Global Fire Emissions Database, Version 4.1s; Randerson et al., 2018). The annual
168 total emissions and global distributions of WACCM simulations agree well with those from
169 FINNv2.5 and GFED4.1s (Figures S1 and S2). The annual total fire carbon emissions during 2015-
170 2019 estimated from the WACCM simulations (2.5 PgC/yr) fall into the range of GFED4.1s (2.0
171 PgC/yr) and FINNv2.5 (3.8 PgC/yr).

172 2.3 SSPs and geoengineering scenarios

173 The Scenario Model Intercomparison Project (ScenarioMIP) based on SSPs is the primary
174 activity within CMIP6 that provides multi-model climate projections based on alternative
175 scenarios (O'Neill et al., 2016). These climate projections are driven by SSP scenarios and are
176 related to the Representative Concentration Pathways (RCPs) as described below. The Land Use
177 Model Intercomparison Project (LUMIP) also provides LULCC data for SSPs (Lawrence et al.,
178 2016, Hurtt et al., 2020). In this study, the SSP1-2.6, SSP2-4.5, SSP3-7.0, and SSP5-8.5 scenarios
179 (O'Neill et al., 2016) are shown. (1) SSP1-2.6 (sustainable development) is the low end of the
180 range of future forcing pathways in SSP and updates the RCP2.6 scenario. SSP1 includes
181 substantial land use change, particularly with increasing global forest cover. (2) SSP2-4.5 is a
182 scenario that represents the middle part of the range of future forcing pathways and updates the
183 RCP4.5 scenario. Land use and aerosol changes in SSP2 (middle-of-the-road development) are
184 not extreme relative to other SSPs. (3) SSP3-7.0 is a scenario with both substantial land use
185 changes (particularly decreased global forest cover) and high near-term climate forcings emissions,
186 particularly sulfur dioxide (SO₂). (4) SSP5-8.5 is the unmitigated baseline scenario, representing
187 the high end of the range of future pathways, and updates the RCP8.5 scenario. There is relatively
188 little land-use change in the 21st century in this scenario which leads to slow decline in the rate of
189 deforestation (O'Neill et al., 2017).

190 The Geoengineering MIP Phase 6 (GeoMIP6) proposed experiments for future projection with
191 geoengineering measures implemented based on ScenarioMIP. In this study we also analyze the
192 response of wildfires under two of the geoengineering experiments – G6Sulfur and G6Solar
193 (Kravitz et al., 2015). Both of these geoengineering scenarios aim to reduce globally-averaged
194 forcing from the ScenarioMIP Tier 1 high-forcing scenario (SSP5-8.5), which averages 8.5 W/m²
195 of forcing by 2100, to the medium-forcing scenario (SSP2-4.5), which averages 4.5 W/m² of
196 forcing by 2100. The geoengineering scenarios were designed to match the surface temperature of
197 SSP2-4.5. G6Sulfur reduces forcing with stratospheric sulfate aerosols. In G6Sulfur experiment,
198 SO₂, the precursor of stratospheric sulfate aerosol has been continuously injected into the model
199 at 25 km altitude at the Equator with the goal of reducing the magnitude of the net anthropogenic
200 radiative forcing and reaching surface temperatures at SSP2-4.5 levels. G6Solar uses the same
201 setup as G6sulfur, but uses solar irradiance reduction to reduce the magnitude of the net
202 anthropogenic radiative forcing. The reduction of the solar constant in G6Solar and the injected
203 SO₂ in G6Sulfur is determined by a feedback algorithm described in Kravitz et al. (2017) and used
204 in Tilmes et al. (2018, 2020). The feedback algorithm identifies differences in the global mean
205 surface temperature between the simulated and the prescribed target temperature each year and
206 from that calculates required changes in the solar constant or SO₂ injections.

207 2.4 Simulations

208 In this study we analyze results from fully coupled WACCM6 simulations for future projection
209 under the aforementioned scenarios from GeoMIP and ScenarioMIP. The continuous long-term
210 (2015 to 2100) simulations used in this study provide a continuous picture of future fire changes
211 and allow us to investigate when and how major changes in the fire trends occur. The horizontal
212 resolution for land and atmosphere is 1.25° × 0.9° (longitude × latitude). Multiple simulations (2~5
213 members) are conducted for each scenario except for the SSP1-2.6 and SSP3-7.0 scenarios (see
214 Table S1 for ensemble sizes). Different ensemble sizes could result in differences in ensemble

215 spread. To be consistent, for scenarios with multiple simulations, only ensemble means are shown
216 and analyzed. I.e., ensemble means are calculated before any analyses or calculations, and hence
217 a scenario with multiple simulations is treated in the same way as a scenario with only one
218 simulation by only using the mean value of the ensemble members. Comparing results from a
219 single simulation to multi-member averages could introduce potential uncertainties as ensemble
220 mean values are in general different from values from a single member. However, the analyses
221 and comparisons here are as useful as comparing single simulations, if not more, because in our
222 approach we attempted to improve model projection for several scenarios by using ensemble
223 means to replace single simulation values when possible. However, the analyses and comparisons
224 here are as useful as comparing single simulations, if not more. The future projection simulations
225 analyzed in this study were initialized with the ensemble WACCM6 historical simulations.
226 Therefore, the initial conditions of different ensemble members are different. Future climate under
227 these simulations has been analyzed in Meehl et al. (2020) and Jones et al. (2020).

228 **3 Future trends of fires**

229 **3.1 Future trends of burned area and fire carbon emissions under the SSP scenarios**

230 The global total wildfire burned area in these simulations is projected to increase under all
231 the SSP scenarios (Figure 1a). The largest increases (averages for the 2091-2100 period relative to
232 the 2021-2030 period) in the global burned area are seen in the SSP5-8.5 scenarios (~20%). The
233 changes in SSP1-2.6 and SSP2-4.5 are less than 4% (see Table S2 for projected regional and global
234 change of burned area and fire carbon emissions in 2091-2100 relative to 2021-2030 (%) under
235 different scenarios). In terms of the spatial distribution, the 40°N–70°N latitude is the only latitude
236 band in which the burned area consistently increases under all the SSP scenarios (Figure 1b). In
237 the 10°S–5°N latitude band (tropical region), the burned area consistently decreases under all
238 scenarios to a diverse extent. While global total burned area is expected to increase under most
239 global warming scenarios, burned area may decrease in some regions due to changes in
240 anthropogenic activities or reduced 2-m relative humidity and/or reduced soil moisture. A more
241 detailed discussion on future trends of fire activity under the SSP scenarios are provided in the
242 Supplement.

243 **3.2 Future trends of burned area and fire carbon emissions with geoengineering**

244 The two geoengineering scenarios (G6Sulfur and G6Solar) are based on SSP5-8.5 and
245 targeted SSP2-4.5. As G6Sulfur reduces the forcing through stratospheric sulfate aerosols while
246 G6Solar directly decreases total incoming solar irradiance, the difference between the two provides
247 insight on the other impacts of sulfate aerosols on fires besides the forcing change. Even though
248 fire carbon emissions are largely driven by burned area, they are also impacted by fuel availability
249 and combustion completeness. Therefore, the fire carbon emissions generally show trends
250 consistent with burned area, with some notable differences. Both burned area and fire carbon
251 emissions under the two geoengineering scenarios are lower than those under SSP5-8.5 (Figures
252 2a and 2c). Lower fire activity in these geoengineering scenarios than SSP5-8.5 is expected due to
253 reduced surface warming towards SSP2-4.5 target climate conditions. However, we found that by
254 the end of the century, the two geoengineering scenarios have lower burned area and fire carbon
255 emissions than not only their base-forcing scenario SSP5-8.5 but also the targeted-forcing scenario
256 SSP2-4.5 (Figures 2a and 2c; see Table S3 for averages of regional and global annual projected

257 burned area (Mha/year) and fire carbon emissions in 2091-2100 under different scenarios). The
258 change of the two geoengineering scenarios compared to SSP2-4.5 in the last decade of the century
259 is small in burned area (-2% for G6Solar and -12% for G6Sulfur) but relatively large in fire carbon
260 emissions (-18% for G6Solar and -23% for G6Sulfur). However, when compared to SSP5-8.5, the
261 reduction of the two geoengineering scenarios in burned area (-18% for G6Solar and -26% for
262 G6Sulfur) is similar to that in fire carbon emissions (-20% for G6Solar and -26% for G6Sulfur).
263 This implies that the difference in fire carbon emissions between the two geoengineering scenarios
264 and SSP2-4.5 are less driven by burned area and that fuel availability plays a more important role
265 in this comparison, while for the difference to SSP5-8.5, changes in burned area plays more of a
266 role in emission differences. The two geoengineering approaches (G6solar and G6sulfur) generally
267 lead to reduced fire activity compared to SSP5-8.5 in most regions in 2091-2100, except for
268 Northern Hemisphere Africa and Equatorial Asia (Figures S3 and S4). When comparing the period
269 2091-2100 to the period 2021-2030, the largest decrease in global total wildfire burned area is seen
270 in the G6sulfur scenario among all the scenarios in this study (~ -11%; see Table S2).

271 In the 40°N–70°N latitude band, the burned area consistently increases under not only all
272 the SSP scenarios but also the two geoengineering scenarios when comparing the period 2091-
273 2100 to the period 2021-2030 (Figure 2b). However, the increase in burned area is lower in the
274 two geoengineering scenarios compared to SSP5-8.5 and is similar to the SSP2-45 scenario. In the
275 -20°S–0° latitude band, the reduction in burned area is larger under G6sulfur than that under
276 G6Solar (Figure 2a). Generally, G6sulfur has a stronger fire-reducing effect than G6solar, with
277 exceptions such as over Europe. We also found notable differences between the two
278 geoengineering methods for some specific regions, implying that the geoengineering method
279 chosen could be inequitable for some countries. For example, G6Solar is the better choice for
280 producing less burned area in Europe, while over Southern Hemisphere Africa, G6Sulfur is better
281 than G6Solar (see Figure S4).

282 **4 Mechanism of geoengineering impacting fires**

283 The two SSP5-8.5-based geoengineering scenarios successfully reduce the radiative
284 forcing from 8.5 Wm⁻² (as in SSP5-8.5) to 4.5 Wm⁻² (as in SSP2-4.5) in 2100 and global surface
285 temperatures between SSP2-4.5 and the two geoengineering scenarios are nearly the same.
286 However, both geoengineering scenarios produce less fire than SSP2-4.5 by 2100 (Figures 2 and
287 3). There are different processes involved in the cooling in G6Sulfur (due to the stratospheric
288 sulfate aerosols) and the cooling in G6Solar (due to directly reduced insolation) (Vioni et al.,
289 2021a). Because of the difference in the resulting climate response, these two geoengineering
290 approaches impact fires differently, even though they are designed to achieve the same forcing
291 level by 2100. Previous studies indicate that stratospheric heating caused by aerosols can impact
292 precipitation and temperature at the surface through alterations to stratospheric dynamics (Jiang et
293 al., 2019; Simpson et al., 2019; Richter et al., 2017; Vioni et al., 2020). Last but not least, the
294 two geoengineering approaches also result in different outcomes for other quantities important for
295 fires. For example, enhanced stratospheric aerosol burden results in changes in direct to diffuse
296 light which promotes plant growth (e.g., Xia et al., 2017; Xu et al., 2020). On the other hand, it
297 can reduce in the hydrological cycle and regional precipitation changes due to the aerosol heating
298 effects in the lower tropical stratosphere (e.g., Tilmes et al., 2013, Simpson et al., 2019).

299 Here we analyze the key variables in the Earth system that are involved in the processes
300 from the reduced insolation on the top of the atmosphere and sulfate aerosols in the stratosphere
301 to fires at the surface. Note that hereafter for a scenario with multiple ensemble members, only the
302 ensemble mean is analyzed and shown. The key variables shown in this section are selected via
303 comparing the key variables that determine fire activity in the fire scheme in CESM2/CLM5 with
304 the key climate variables that are impacted by geoengineering approaches. The analyses are
305 conducted for 14 individual fire regions following Giglio et al. (2010), namely Boreal North
306 America, Temperate North America, Central America, Northern Hemisphere South America,
307 Southern Hemisphere South America, Europe, Middle East, Northern Hemisphere Africa,
308 Southern Hemisphere Africa, Boreal Asia, Central Asia, Southeast Asia, Equatorial Asia, and
309 Australia and New Zealand (Figure S3).

310 **4.1 Surface temperature**

311 Even though the mean surface temperature (TS) for the whole globe and the land are similar
312 under the two geoengineering scenarios and SSP2-4.5 (Figure 4), regional differences exist
313 (Figures 5). For example, over Equatorial Asia, the annual surface mean temperatures in the two
314 geoengineering scenarios are consistently lower than that in SSP2-4.5 by $\sim 0.3\text{K}$ during 2091-2100
315 (Figure S6). The spatial distribution of burned area difference and fire carbon emission difference
316 between G6Solar/G6Sulfur and SSP5-8.5 (Figure 3) are not always co-located with their spatial
317 distribution of surface temperature difference (Figure 5). To understand to what extent the surface
318 temperature drives fire activity change, we calculate correlations of surface temperature change
319 and burned area/fire carbon emission change for individual fire regions under SSP2-4.5, G6Solar,
320 and G6Sulfur. Surface temperature change (ΔTS) for a given region is calculated based on the
321 individual model grids within the region and annual values between 2091-2100. It is defined as
322 the difference between the analyzed scenario (i.e., G6Solar, G6Sulfur, and SSP2-4.5) and the
323 reference scenario (i.e., SSP5-8.5). Burned area change (ΔBA) and fire carbon emission change
324 (ΔCemis) are defined in the same way. For example, if a region consists of 500 individual model
325 grids, as we use 10 years of annual data, there will be 5000 (500×10) pairs of ΔTS and ΔBA to
326 calculate correlations. The correlations calculated here account for spatial variability within the
327 region and interannual variability during 2091-2100.

328 Overall, surface temperature plays a more important role in the decrease of fire activity in
329 the two geoengineering scenarios compared to that in SSP2-4.5 relative to SSP5-8.5 (Figure 6).
330 This is expected because the only difference between the two geoengineering scenarios and SSP5-
331 8.5 is the specific application of climate intervention; whereas the differences between SSP2-4.5
332 and SSP5-8.5 involves several other differences including population growth and LULCC. For
333 G6Solar and G6Sulfur, the strongest impact of surface temperature change on burned area occurs
334 over Southern Hemisphere South America (correlation=0.42 for G6Solar and 0.45 for G6Sulfur),
335 followed by Southern Hemisphere Africa, Temperate North America, and Europe. The impact of
336 surface temperature change over boreal regions (Boreal North America and Boreal Asia) are
337 relatively small. This suggests that the changes in area burnt in these regions might be
338 predominantly driven by other factors changed by geoengineering (e.g., hydrological cycle) rather
339 than the surface temperature changes, which will be analyzed in the following sub-sections. For
340 G6Solar and G6Sulfur, the impact of surface temperature on burned area is generally larger than
341 its impact on fire carbon emissions. This is expected as fire carbon emissions in
342 CESM2/WACCM6 are determined by burned area together with vegetation characteristics (carbon

343 density and combustion completeness; Li et al., 2012), which introduces more uncertainties. The
344 only exception occurs over the Northern Hemisphere South America where surface temperature
345 plays a more important role in fire carbon emissions than burned area for not only G6Solar
346 (correlation is 0.37 versus 0.29) and G6Sulfur (correlation is 0.37 versus 0.24) but also SSP2-4.5
347 (correlation is 0.40 versus 0.23). Over Northern Hemisphere South America, the correlations
348 between ΔTS and $\Delta BA/\Delta Cemis$ are also close under the three scenarios. Since combustion
349 completeness is a fixed parameter, this difference points to the possibility that the reduced surface
350 temperature has a larger impact on carbon density over Northern Hemisphere South America than
351 over other regions.

352 Overall, we find that the surface temperature change introduced by the two geoengineering
353 approaches (solar irradiance reduction and stratospheric sulfate aerosols) by the end of the century
354 impacts burned area and fire carbon emissions, e.g., the introduced cooling results in smaller fire
355 activity. The degree of impact varies dramatically across different regions. The impact of surface
356 temperature in G6Solar and G6Sulfur are overall close. However, surface temperature alone does
357 not account for all the changes in fire activity.

358 4.2 Precipitation

359 Precipitation change is also an important consequence of climate change and
360 geoengineering (Figure 4). Global precipitation is expected to increase under climate change as
361 higher tropospheric temperature leads to more moisture in the air. Previous studies found that
362 geoengineering could eliminate these increases in precipitation and can even reduce global mean
363 or regional precipitation relative to the target scenario, depending on the geoengineering approach
364 (Tilmes et al., 2013, Simpson et al., 2019, Vioni et al., 2021a). The spatial distribution of
365 precipitation changes under G6Solar and G6Sulfur relative to SSP5-8.5 are similar (Figure 5). The
366 trend of precipitation varies dramatically across regions (Figure S7). Precipitation is also important
367 for fires. Precipitation itself could have either a positive or a negative impact on future fires
368 because precipitation can impact both fuel combustibility and fuel availability, which impact fire
369 in opposite directions. In addition, precipitation changes can also lead to changes in relative
370 humidity and soil water content, which are important factors for fires. Here we apply the same
371 analyses for precipitation change ($\Delta Precip$) as in Section 4.1 for surface temperature change (ΔTS).

372 The reduction in precipitation by geoengineering has the opposite impact on fire as the
373 reduction in surface temperature by geoengineering, as shown by the negative correlations of
374 $\Delta Precip$ and $\Delta BA/\Delta Cemis$ (Figure 6). The correlations are consistently negative across all the
375 scenarios (G6Solar, G6Sulfur, and SSP2-4.5) and almost all regions. The largest impact of
376 precipitation change occurs over Equatorial Asia for all three scenarios (correlation is -0.45–0.42
377 for ΔBA and -0.43–0.33 for $\Delta Cemis$), which is aligned with the strong precipitation change over
378 the region (Figures 5). Over the Middle East, precipitation change has a relatively large impact on
379 burned area and fire carbon emissions under G6Solar as well as SSP2-4.5, however the impact is
380 small under G6Sulfur. We note that unlike the impact of ΔTS , the impact $\Delta Precip$ is relatively
381 large over boreal regions. We conduct a sensitivity test of 1-year lag correlation (see Table S4 for
382 the correlation values) to understand the impact of previous year precipitation change on fire
383 activity (for example calculating correlation of $\Delta Precip$ for 2091 and $\Delta BA/\Delta Cemis$ for 2092). We
384 found that this correlation is still significant for most regions, though it is generally lower. Overall
385 precipitation change is inversely related to burned area change and fire carbon emission change.

386 Therefore, for these regions where precipitation is reduced compared to SSP5-8.5 as a consequence
387 of geoengineering such as Equatorial Asia, the reduction in burned area and fire carbon emissions
388 due to reduced surface temperature are offset to some extent.

389 4.3 Humidity

390 Humidity is also impacted by geoengineering. The future trends of specific humidity (g/kg)
391 and relative humidity (%) are opposite as specific humidity is projected to increase while relative
392 humidity is projected to decrease compared to SSP5-8.5 (Figure 4). Their spatial distribution and
393 inter-scenario differences are also divergent (Figures 4 and 5). This is due to the fact that relative
394 humidity is driven by not only the actual moisture content but also the temperature. The same
395 amount of water vapor results in a higher relative humidity in colder air than in warm air. Therefore
396 a reduction in relative humidity in a warming climate indicates that the relative amount of water
397 vapor has not increased proportional to the warming. Relative humidity is a driving variable in the
398 CLM5 fire module in multiple places (e.g., lower relative humidity leads to higher fuel
399 combustibility and larger fire spread). Here we focus our analysis on the relative humidity change
400 at 2-meter (ΔRH) as relative humidity is directly used in the CLM5 fire module. Changes in
401 relative humidity show different spatial distribution between the G6solar minus SSP5-8.5 and
402 G6sulfur minus SSP5-8.5 (Figure 5), even though their global average values are close (Figure 4).

403 The relative humidity change (ΔRH) is negatively correlated to $\Delta BA/\Delta C_{emis}$ across all
404 scenarios and regions (Figure 6). Therefore, the higher relative humidity in G6Solar, G6Sulfur,
405 and SSP2-4.5 than SSP5-8.5 (Figure 4) leads to less fire activity globally. Overall, the relative
406 humidity change is more strongly correlated to $\Delta BA/\Delta C_{emis}$, indicating that relative humidity
407 change is a more important driver of fire activity change under geoengineering than surface
408 temperature or precipitation.

409 4.4 Wind speed

410 Wind speed is also an important driving factor in fire spread and is also indirectly impacted
411 by geoengineering (Figure 4). In CLM5, wind speed is used in the calculation of fire spread and
412 hence burned area. Wind speed mainly has an indirect impact on fire carbon emissions through
413 burned area. Here we analyze 10-meter wind speed (U_{10}). By the end of the century, SSP2-4.5
414 has slightly higher U_{10} than SSP5-8.5, G6Solar has similar U_{10} as SSP5-8.5, while G6Sulfur has
415 slightly lower U_{10} than SSP5-8.5 over land (Figure 4). However, the regional difference can be
416 relatively large (Figures 5). G6sulfur and G6solar have significantly different U_{10} over Southern
417 Hemisphere ocean (Figures 5). However, the difference in U_{10} between G6solar and G6sulfur
418 over land is relatively small with exceptions such as over Australia and Northern Hemisphere
419 Africa where G6sulfur has lower U_{10} .

420 Wind speed change has consistently positive correlations with changes in burned area and
421 fire carbon emissions under the two geoengineering scenarios across all analyzed regions (which
422 is not the case for SSP2-4.5, where ΔU_{10} is negatively correlated ΔBA or ΔC_{emis} over most
423 regions). This indicates that the reduction in wind speed as a byproduct of geoengineering (Figure
424 4) leads to less fire activity globally. The wind speed reduction is relatively large over South
425 Hemisphere Africa (Figure 5), and the correlations are also high, indicating the wind speed
426 reduction is partially responsible for the reduction in fire activity over South Hemisphere Africa.

427 4.5 Soil water content

428 Soil water content is a key driver of fire activity as it impacts fuel combustibility and fire
429 spread. Soil water content is indirectly impacted by the geoengineering approaches through the
430 hydrological cycle. The precipitation changes as a result of geoengineering compared to SSP5-8.5
431 strongly impacts the soil water content, and the soil water content further drives the relative
432 humidity near the surface through evapotranspiration. We see a much smaller reduction in soil
433 water content in the geoengineering runs compared to SSP2-45. Therefore, the future trends of soil
434 water content (here we use the model variable SOILWATER_10CM, i.e., the soil water content in
435 the top 10 cm (kg/m^2) to evaluate soil moisture) are close to the future trends of relative humidity
436 (Figure 4) globally. However, in the last decade of the century, difference in soil water content
437 among the scenarios is larger than the difference in relative humidity among the scenarios (the
438 difference of the 3 scenarios from SSP5-8.5 are $\sim 1\text{--}2\%$ for relative humidity and $\sim 4\text{--}7\%$ for
439 SOILWATER_10CM). Here we include analyses of soil water content not only because it is a
440 very important driver of fire activity but also because the spatial distributions of soil water change
441 ($\Delta\text{SOILWATER}$) can be different than relative humidity change in some regions (Figures 5).
442 Overall, similar to precipitation and relative humidity, soil water content change is negatively
443 related to burned area and fire carbon emissions with different spatial distributions (Figure 6). For
444 example, over the boreal regions and Europe, the impact of $\Delta\text{SOILWATER}$ is smaller than the
445 impact of ΔRH , while over Central Asia it is larger.

446 4.6 Others

447 There are other relevant variables that are not analyze in detail here. For example, the
448 reduction in the downwelling solar flux at the surface (ΔFSDS) is a direct consequence of
449 geoengineering (solar irradiance reduction and stratospheric sulfate aerosols). In addition, water
450 vapor content and cloud change as a consequence of geoengineering also impact downwelling
451 solar flux at the surface. We include the analyses of downwelling solar flux in the supplement
452 (Figures S8-S9) as the downwelling solar flux at the surface does not directly determine burned
453 area and fire carbon emissions in the model. The downwelling solar flux at the surface is positively
454 related to burned area and fire carbon emissions. Therefore, the lower downwelling solar flux at
455 the surface than SSP5-8.5 as a result of the geoengineering approaches leads to less fires globally
456 while the higher downwelling solar flux at the surface under SSP2-4.5 than SSP5-8.5 tends to
457 increase fire activity and can offset the overall reduction fires in SSP2-4.5 than SSP5-8.5 to some
458 degree. As another example, vegetation carbon can also impact the total fire carbon emissions and
459 are also impacted by fire activity. However, we do not further analyze the impact of fuel load
460 because geoengineering approaches do not seem to change global total fuel load significantly. The
461 future trend of total vegetation carbon under G6Solar and G6Sulfur are very close to SSP5-8.5,
462 and the three of them are different from SSP2-4.5 as total vegetation carbon is largely driven by
463 CO_2 (Figure 4).

464 4.7 G6Sulfur versus G6Solar

465 Comparisons between G6Sulfur and G6Solar provide insight on the potential impact of
466 stratospheric sulfate aerosols on fires other than the intended climate intervention. In general, using
467 sulfur to create climate control enhances the effect of the solar management on the modeled fire
468 response. While both geoengineering approaches show strongest inverse relationships between fire

469 parameters and relative humidity and soil moisture, G6Sulfur shows smaller reductions in these
470 climate variables than G6Solar. Globally, G6Sulfur has lower burned area and fire carbon
471 emissions than G6Solar by the end of the century. The differences between G6Sulfur and G6Solar
472 varies regionally (Figures 7a-7b). For example, over most regions, G6Sulfur has less fire activity
473 than G6Solar whereas over Europe, G6Sulfur has more fire activity than G6Solar, which is related
474 to the warming over Northern Eurasia caused by G6Sulfur (Figure 7c) and a positive correlation
475 between BA and surface temperature over Europe. However, we note that two ensemble members
476 may not fully reflect the robust signal. The spatial distributions of differences between G6Sulfur
477 and G6Solar in burned area and fire carbon emissions (Figures 7a-7b) are close to the spatial
478 distributions of difference between G6Sulfur and G6Solar in relative humidity (Figure 7e) and soil
479 water content (Figure 7g). G6Sulfur has higher relative humidity and soil water content over most
480 regions. However, over Europe relative humidity and soil water content in G6Sulfur are lower than
481 those in G6Solar, which is consistent with what has been found in burned area and fire carbon
482 emissions. In addition, over South America, the distribution of difference in relative humidity and
483 soil water content is similar to the distribution of difference in burned area and fire carbon
484 emissions. This indicate that the differences in future fire activity between the two geoengineering
485 approaches is likely driven by relative humidity and soil water content.

486 A summary of the relationships between Δ BA and the changes in the related variables (Δ TS,
487 Δ Precip, Δ RH, Δ U10, Δ SOILWATER, and Δ FSDS) for G6Sulfur versus G6Solar is shown in
488 Figure 8 (note that Δ BA as well as Δ of other variables are calculated by the difference of the
489 geoengineering run from the reference case, i.e., SSP5-8.5). Overall, the impacts of these driving
490 variables are similar in the two geoengineering approaches (as the points fall close to the diagonal).
491 However, these variables in general have larger impacts on burned area in G6Solar than in
492 G6Sulfur (as the majority of the points fall in the shaded area where the x-axis value is larger than
493 the y-axis value). It is possible that stratospheric sulfate aerosols could yield to additional changes
494 such as higher diffuse radiation that benefits plant growth, which reduces the correlations of the
495 analyzed factors with fires.

496 4.8 Discussion

497 The key finding of this study is that fire burned area and emissions are lower in the
498 geoengineering runs than not only SSP5-8.5 but also the target SSP2-4.5 run in CESM2/WACCM6.
499 Here we analyze the key climate variables that are largely and/or directly impacted by the two
500 geoengineering approaches and are important drivers of fires. A summary of the relationships
501 between Δ BA and the change in the related variables (Δ TS, Δ Precip, Δ RH, Δ U10, Δ SOILWATER,
502 and Δ FSDS) versus the relationships between Δ Cemis and the change in the related variables for
503 G6Solar, G6Sulfur, and SSP2-4.5 are shown in Figure 9. The future trends of the analyzed
504 variables and their changes from SSP5-8.5 can be opposite over different regions. However, the
505 directions of impact (i.e., positive or negative correlation) are overall consistent across the 14 fire
506 regions and 3 scenarios. Therefore the dominant factors are also different across regions.

507 We note that under both geoengineering scenarios, changes in relative humidity, soil water,
508 and downwelling solar flux at the surface all have strongest impacts over Equatorial Asia (as
509 shown by strongest correlations among the 14 regions; Figure 9). Changes in wind speed and
510 precipitation also have relative strong impacts over Equatorial Asia compared to other regions.
511 Overall, Equatorial Asia is the most sensitive to the climate variable changes introduced by both

512 geoengineering approaches (Figure 9), even though the resulting fire activity changes over
513 Equatorial Asia are not as strong as some other regions (Figure 3) likely due to the relatively weak
514 change in the climate variables (e.g., Figures 5). On the contrary, Boreal North America is not
515 sensitive to most of the climate variable changes introduced by both geoengineering approaches
516 (the correlations are the lowest and close to 0, Figure 9), which is likely the reason why the 40°N–
517 70°N latitude band is the only latitude band in which the zonal mean burned area consistently
518 increases even under the geoengineering scenarios (Figures 1 and 2). Boreal Asia is similar to
519 Boreal North America with the correlations overall being slightly stronger.

520 For G6Solar and G6Sulfur, the correlations of the shown variables (especially for Δ TS,
521 Δ RH, Δ U10, and Δ FSDS) with burned area are in general stronger than their correlations with fire
522 carbon emissions (as shown by more data points that fall into the shaded area). This is expected
523 because these variables directly impact burned area, whereas fire carbon emissions are determined
524 by both burned area and fuel availability. Fuel availability is further directly or indirectly impacted
525 by many variables including but not limited to the shown ones here. Therefore, the correlations
526 between the shown variables with fire carbon emissions are not as strong as their correlations with
527 burned area. The patterns in G6Solar and G6Sulfur are closer to each other when using SSP2-4.5
528 as a reference (Figures 6). This is not only because their approaches to reducing forcing from
529 SSP5-8.5 to 4.5 W/m² are different, but also because the scenario configuration of SSP2-4.5 is
530 different from SSP5-8.5 and SSP5-8.5-based G6Solar and G6Sulfur (e.g., LULCC).

531 The analyses above (Sections 4.1-4.7) use SSP5-8.5 as the reference case to calculate the
532 changes (Δ) because the two geoengineering scenarios are based on SSP5-8.5, and their difference
533 is only due to the geoengineering approaches. Here we also include analyses that uses the target
534 SSP2-4.5 as the reference case in the Supplement (Figures S12). The signs of the correlations are
535 in general consistent whether SSP5-8.5 or SSP2-4.5 is used as the reference case (Figures S11-
536 S12). For example, even though relative humidity change from SSP2-4.5 are very different
537 regionally under G6Solar and G6Sulfur (Figure 5), the signs of the correlations are consistently
538 negative over all regions and under the two geoengineering scenarios. In general, the impacts of
539 the analyzed variables on changes of the burned area and fire carbon emissions from SSP2-4.5 are
540 weaker (Figures S11-S12), likely due to the fact that the changes (Δ) between the two
541 geoengineering scenarios and SSP2-4.5 are due to not only geoengineering introduced climate
542 variable changes (e.g., surface temperature, relative humidity, soil water content, etc.) but also
543 other factors such as atmospheric CO₂ and LULCC.

544 **4.9 Uncertainty and limitation**

545 We recognize that there are several limitations in this study. For example, even though
546 CESM2 is a state-of-the-art model, uncertainties and limitations exist in the model
547 parameterizations (including the parameterization of fire-related processes and the lack of
548 interactive fire emissions). In addition, the fire emissions of trace gases and aerosols are not fully
549 coupled, as CESM2 uses the CMIP6 fire emission inventories. This study analyzes results from
550 only one model (CESM2) and similar studies need to be conducted with other models to test inter-
551 model consistency. Lastly, there are only two ensemble members in each geoengineering scenario,
552 which can lead to larger variability at regional scale in particular resulting in large uncertainties in
553 the response of geoengineering on rainfall with implications of other relevant variables. While
554 largescale changes are significant, a larger ensemble size in future study will reduce uncertainties

555 in the regional results. More studies are needed to fully understand the future trends of fires and
556 the impact of geoengineering on fires.

557 **5. Conclusions**

558 Here we analyzed the future fires under geoengineering as well as SSP scenarios, and
559 assess how the different geoengineering approaches impact fires. The major conclusions and
560 implications are as follows:

561 (1) The global total wildfire burned area is projected to increase under the unmitigated scenario
562 (SSP5-8.5), and decrease under the two geoengineering scenarios (solar irradiance reduction and
563 stratospheric sulfate aerosols) comparing the averages of 2091-2100 relative to 2021-2030.

564 (2) By the end of the century, the two geoengineering scenarios exhibit lower burned area and fire
565 carbon emissions than not only their base-forcing scenario (SSP5-8.5) but also the targeted-forcing
566 scenario (SSP2-4.5).

567 (3) The two geoengineering approaches (solar irradiance reduction and stratospheric sulfate
568 aerosols) generally lead to less wildfire activity in most regions in 2091-2100, except for the
569 Northern Hemisphere Africa and Equatorial Asia. The 40°N–70°N latitude band is the only
570 latitude band in which the zonal mean burned area consistently increases under all the scenarios,
571 even the geoengineering scenarios.

572 (4) Overall, changes of G6Solar and G6Sulfur from SSP5-8.5 in surface temperature, wind speed,
573 and downwelling solar flux at the surface are positively correlated to the changes in burned area
574 and fire carbon emissions, while their changes in precipitation, relative humidity, and soil water
575 content are negatively correlated to the changes in burned area and fire carbon emissions.

576 (5) Generally, the stratospheric sulfate aerosols approach has a stronger fire-reducing effect than
577 the solar irradiance reduction approach. The impacts of the analyzed variable changes are generally
578 larger (percent-wise) on burned area than fire carbon emissions.

579 (6) Geoengineering imposed reduction in surface temperature and wind speed, and increase in
580 relative humidity and soil moisture, reduce fires by the end of the century. However, the reduction
581 in precipitation resulting from geoengineering offsets its overall fire-reducing effect to some extent.

582 The success of future fire mitigation with the two geoengineering approaches in the
583 CESM2/WACCM6 model results is encouraging. However, this study is not a closure study due
584 to the uncertainties and limitations (Section 4.9). More research is needed for this topic. Here we
585 do not indicate that fewer fires under the geoengineering approaches are definitively beneficial.
586 After all, fire is a natural process and a key component of the dynamic Earth system, and wildfires
587 were present long before anthropogenic activities. Lastly, fire risk increase is only one of many
588 possible consequences of climate change, and fire activity reduction is also only one of many
589 possible consequences of climate intervention. We present this study only as a reference for the
590 future when geoengineering is considered.

591 **Data availability**

593 The simulation data used in this study are archived on the Earth System Grid Federation (ESGF)
594 (<https://esgf-node.llnl.gov/projects/cmip6>; last access: 12 December 2022). The model Source ID
595 is CESM2-WACCM for CESM2-WACCM6. FINN2.5 data are available at:

596 <https://www.acom.ucar.edu/Data/fire/>. GFED data are available at:
597 <https://www.globalfiredata.org/>.

598

599 **Author contributions**

600 WT led the analysis with the contribution from ST. ST and DML contributed to the interpretation
601 of the model results. WT prepared the paper with improvements from ST, DML, FL, CH, LKE,
602 RRB, and LX.

603

604 **Acknowledgements**

605 This material is based upon work supported by the National Center for Atmospheric Research,
606 which is a major facility sponsored by the National Science Foundation under Cooperative
607 Agreement No. 1852977. W. Tang was supported by NCAR Advanced Study Program
608 Postdoctoral Fellowship. We thank the reviewers for their helpful comments that improves this
609 manuscript. W. Tang thanks Wangcai Bao (Syrian hamster; Sep 8, 2020 – Jul 22, 2022) for his
610 support during the pandemic.

611

612

613

614 **References**

615 Abatzoglou, J. T., Williams, A. P., & Barbero, R. (2019). Global emergence of anthropogenic
616 climate change in fire weather indices. *Geophysical Research Letters*, 46(1), 326-336.

617 Andela, N. and van der Werf, G.R., 2014. Recent trends in African fires driven by cropland
618 expansion and El Nino to La Nina transition. *Nature Climate Change*, 4(9), pp.791-795.

619 Andela N, Morton DC, Giglio L, Chen Y, Van Der Werf GR, Kasibhatla PS, DeFries RS, Collatz
620 GJ, Hantson S, Kloster S, Bachelet D. A human-driven decline in global burned area. *Science*.
621 2017 Jun 30;356(6345):1356-62.

622 [Bala, et al. \(2008\): Impact of geoengineering schemes on the global hydrological cycle, PNAS,](#)
623 [doi:10.1073/pnas.0711648105.](#)

624 Bowman, D.M., Balch, J.K., Artaxo, P., Bond, W.J., Carlson, J.M., Cochrane, M.A., D'Antonio,
625 C.M., DeFries, R.S., Doyle, J.C., Harrison, S.P. and Johnston, F.H., 2009. Fire in the Earth system.
626 *science*, 324(5926), pp.481-484.

627 Bowman, D. M. J. S., Balch, J. K., Artaxo, P., Bond, W. J., Carlson, J. M., Cochrane, M. A.,
628 D'Antonio, C. M., DeFries, R. S., Doyle, J. C., Harrison, S. P., Johnston, F. H., Keeley, J. E., Ford,
629 B., Val Martin, M., Zelasky, S. E., Fischer, E. V., Anenberg, S. C., Heald, C. L., and Pierce, J. R.:
630 Future Fire Impacts on Smoke Concentrations, Visibility, and Health in the Contiguous United
631 States, *GeoHealth*, 2, 229–247, 2018.

632 Bowman, D. M. J. S., Kolden, C. A., Abatzoglou, J. T., Johnston, F. H., van der Werf, G. R., &
633 Flannigan, M. (2020). Vegetation fires in the Anthropocene. *Nature Reviews Earth & Environment*,
634 1-16.

635 Brey, S. J., Barnes, E. A., Pierce, J. R., Wiedinmyer, C., & Fischer, E. V. (2018). Environmental
636 conditions, ignition type, and air quality impacts of wildfires in the southeastern and western
637 United States. *Earth's Future*, 6(10), 1442-1456.

638 Brey, S. J., Barnes, E. A., Pierce, J. R., Swann, A. L., & Fischer, E. V. Past variance and future
639 projections of the environmental conditions driving western US summertime wildfire burn area.
640 *Earth's Future*, e2020EF001645, 2020.

641 Chen, Y., Morton, D. C., Andela, N., Van Der Werf, G. R., Giglio, L., & Randerson, J. T. (2017).
642 A pan-tropical cascade of fire driven by El Niño/Southern Oscillation. *Nature Climate Change*,
643 7(12), 906-911.

644 Coen, J., Cameron, M., Michalakes, J., Patton, E., Riggan, P., and Yedinak, K.: WRF-Fire:
645 Coupled weather-wildland fire modeling with the Weather Research and Forecasting model, *J.*
646 *Appl. Meteor. Climatol.*, 52, 16–38, doi:10.1175/JAMC-D-12-023.1, 2013.

647 Danabasoglu, G., Lamarque, J. F., Bacmeister, J., Bailey, D. A., DuVivier, A. K., Edwards, J.,
648 Emmons, L. K., Fasullo, J., Garcia, R., Gettelman, A., Hannay, C., Holland, M. M., Large, W. G.,
649 Lauritzen, P. H., Lawrence, D. M., Lenaerts, J. T. M., Lindsay, K., Lipscomb, W. H., Mills, M. J.,
650 Neale, R., Oleson, K. W., OttoBliesner, B., Phillips, A. S., Sacks, W., Tilmes, S., van Kampenhout,
651 L., Vertenstein, M., Bertini, A., Dennis, J., Deser, C., Fischer, C., Fox-Kemper, B., Kay, J. E.,
652 Kinnison, D., Kushner, P. J., Larson, V. E., Long, M. C., Mickelson, S., Moore, J. K., Nienhouse,
653 E., Polvani, L., Rasch, P. J., and Strand, W. G.: The Community Earth System Model Version 2
654 (CESM2), *J. Adv. Model. Earth Syst.*, 12, 1–35, <https://doi.org/10.1029/2019MS001916>, 2020.

655 Di Virgilio, G., Evans, J. P., Blake, S. A. P., Armstrong, M., Dowdy, A. J., Sharples, J., & McRae,
656 R.: Climate change increases the potential for extreme wildfires. *Geophysical Research Letters*,
657 46, 8517–8526. <https://doi.org/10.1029/2019GL083699>, 2019.

658 Di Virgilio G, Evans JP, Clarke H, Sharples J, Hirsch AL, Hart MA. Climate change significantly
659 alters future wildfire mitigation opportunities in southeastern Australia. *Geophysical Research*
660 *Letters*. 2020 Aug 16;47(15):e2020GL088893.

661 Emmons, L. K., Schwantes, R. H., Orlando, J. J., Tyndall, G., Kinnison, D., Lamarque, J.-F.,
662 Marsh, D., Mills, M. J., Tilmes, S., Bardeen, Ch., Buchholz, R. R., Conley, A., Gettelman, A.,
663 Garcia, R., Simpson, I., Blake, D. R., Meinardi, S., and Pétron, G.: The Chemistry Mechanism in
664 the Community Earth System Model version 2 (CESM2), *J. Adv. Model. Earth Sys.*, 12,
665 e2019MS001882, <https://doi.org/10.1029/2019MS001882>, 2020.

666 Flannigan M, Campbell I, Wotton M, Carcaillet C, Richard P, Bergeron Y. Future fire in Canada's
667 boreal forest: paleoecology results and general circulation model-regional climate model
668 simulations. *Canadian journal of forest research*. 2001 May 1;31(5):854-64.

669 Flannigan, M. D., Krawchuk, M. A., de Groot, W. J. et al.: Implications of changing climate for
670 global wildland fire, *Int. J. Wildland Fire*, 18, 483–507, 2009.

671 Flannigan, M., Cantin, A. S., De Groot, W. J., Wotton, M., Newbery, A., & Gowman, L. M.:
672 Global wildland fire season severity in the 21st century. *Forest Ecology and Management*, 294,
673 54-61, 2013.

674 Ford B, Val Martin M, Zelasky SE, Fischer EV, Anenberg SC, Heald CL, Pierce JR. Future fire
675 impacts on smoke concentrations, visibility, and health in the contiguous United States. *GeoHealth*.
676 2018 Aug;2(8):229-47.

677 Gettelman, A., Mills, M. J., Kinnison, D. E., Garcia, R. R., Smith, A. K., Marsh, D. R., Tilmes, S.,
678 Vitt, F., Bardeen, C. G., McInerny, J., Liu, H.-L., Solomon, S. C., Polvani, L. M., Emmons, L. K.,
679 Lamarque, J.-F., Richter, J. H., Glanville, A. S., Bacmeister, J. T., Phillips, A. S., Neale, R. B.,

680 Simpson, I. R., DuVivier, A. K., Hodzic, A., and Randel, W. J.: The Whole Atmosphere
681 Community Climate Model Version 6 (WACCM6), *Journal of Geophysical Research:*
682 *Atmospheres*, <https://doi.org/10.1029/2019JD030943>, 2019.

683 Girardin MP, Mudelsee M. Past and future changes in Canadian boreal wildfire activity.
684 *Ecological Applications*. 2008;18(2):391-406.

693 Giglio, L., Randerson, J. T., van der Werf, G. R., Kasibhatla, P. S., Collatz, G. J., Morton, D. C.,
694 and DeFries, R. S.: Assessing variability and long-term trends in burned area by merging multiple
695 satellite fire products, *Biogeosciences*, 7, 1171–1186, <https://doi.org/10.5194/bg-7-1171-2010>,
696 2010.

697 Hanes, C. C., Wang, X., Jain, P., Parisien, M. A., Little, J. M., & Flannigan, M. D. (2019). Fire-
698 regime changes in Canada over the last half century. *Canadian Journal of Forest Research*, 49(3),
699 256-269.

700 Huang Y, Jin Y, Schwartz MW, Thorne JH. Intensified burn severity in California’s northern
701 coastal mountains by drier climatic condition. *Environmental Research Letters*. 2020 Sep
702 25;15(10):104033.

703 Hurtt, G.C., L. Chini. R. Sahajpal, S. Frolking, B.L. Bodirsky, K. Calvin, J.C. Doelman, J. Fisk, S.
704 Fujimori, K.K. Goldewijk, T. Hasegawa, P. Havlik, A. Henimann, F. Humpnoder, J. Jungclaus, J.
705 Kaplan, J. Kennedy, T. Kristzin, D. Lawrence, P. Lawrence, L. Ma, O. Mertz, J. Pongratz, A. Popp,
706 B. Poulter, K. Riahi, E. Shevliakova, E. Stehfest, P. Thornton, F.N. Tubiello, D.P. Van Vuuren,
707 and X. Zhang, 2020. Harmonization of Global Land-Use Change and Management for the Period
708 850-2100 (LUH2) for CMIP6. *GMD*, 13, 5425-5464, doi.org/10.5194/gmd-13-5425-2020.

709 Jiang, J., Cao, L., MacMartin, D. G., Simpson, I. R., Kravitz, B., Cheng, W., Visioni, D., Tilmes,
710 S., Richter, J. H., and Mills, M. J.: Stratospheric Sulfate Aerosol Geoengineering Could Alter the
711 High-Latitude Seasonal Cycle, *Geophys. Res. Lett.*, 46, 14153–14163,
712 <https://doi.org/10.1029/2019GL085758>, 2019.

713 Jones, B. and O’Neill, B. C.: Spatially explicit global population scenarios consistent with the
714 Shared Socioeconomic Pathways, *Environ. Res. Lett.*, 11, 4003, <https://doi.org/10.1088/1748-9326/11/8/084003>, 2016.

716 Jones, A., Haywood, J. M., Jones, A. C., Tilmes, S., Kravitz, B., and Robock, A.: North Atlantic
717 Oscillation response in GeoMIP experiments G6solar and G6sulfur: why detailed modelling is
718 needed for understanding regional implications of solar radiation management, *Atmos. Chem.*
719 *Phys. Discuss.*, <https://doi.org/10.5194/acp-2020-802>, in review, 2020.

720 Krawchuk, M. A., Kull, C. A., Marston, J. B., Moritz, M. A., Prentice, I. C., Roos, C. I., Scott,
721 A. C., Swetnam, T. W., van der Werf, G. R., and Pyne, S. J.: Fire in the Earth System, *Science*,
722 324, 481–484, <https://doi.org/10.1126/science.1163886>, 2009.

723 Knorr, W., Arneth, A., and Jiang, L.: Demographic controls of future global fire risk, *Nat. Clim.*
724 *Change*, 6, 781–785, <https://doi.org/10.1038/NCLIMATE2999>, 2016a.

725 Knorr, W., Jiang, L., and Arneth, A.: Climate, CO2 and human population impacts on global
726 wildfire emissions, *Biogeosciences*, 13, 267–282, <https://doi.org/10.5194/bg-13-267-2016>, 2016b.

727 Kravitz, B., Robock, A., Tilmes, S., Boucher, O., English, J. M., Irvine, P. J., Jones, A., Lawrence,
728 M. G., MacCracken, M., Muri, H., Moore, J. C., Niemeier, U., Phipps, S. J., Sillmann, J.,

729 Storelvmo, T., Wang, H., and Watanabe, S.: The Geoengineering Model Intercomparison Project
730 Phase 6 (GeoMIP6): simulation design and preliminary results, *Geosci. Model Dev.*, 8, 3379–3392,
731 doi:10.5194/gmd-8-3379-2015, 2015.

732 Kravitz, B., Lamarque, J.-F., Tribbia, J. J., Tilmes, S., Vitt, F., Richter, J. H., MacMartin, D. G.,
733 and Mills, M. J.: First Simulations of Designing Stratospheric Sulfate Aerosol Geoengineering to
734 Meet Multiple Simultaneous Climate Objectives, *J. Geophys. Res.-Atmos.*, 122, 12616–12634,
735 <https://doi.org/10.1002/2017jd026874>, 2017.

736 Lasslop, G., Hantson, S., Harrison, S. P., Bachelet, D., Burton, C., Forkel, M., Forrest, M., Li F.,
737 Melton, J. R., Yue, C., Archibald, S., Scheiter, S., Arneth, A., Hickler, T., and Sitch, S.: Global
738 ecosystems and fire: Multi-model assessment of fire-induced tree-cover and carbon storage
739 reduction, *Glob. Change Biol.*, 26, 5027–5041, <https://doi.org/10.1111/gcb.15160>, 2020.

740 Lawrence, D. M., Hurtt, G. C., Arneth, A., Brovkin, V., Calvin, K. V., Jones, A. D., Jones, C. D.,
741 Lawrence, P. J., de Noblet-Ducoudré, N., Pongratz, J., Seneviratne, S. I., and Shevliakova, E.: The
742 Land Use Model Intercomparison Project (LUMIP) contribution to CMIP6: rationale and
743 experimental design, *Geosci. Model Dev.*, 9, 2973–2998, [https://doi.org/10.5194/gmd-9-2973-](https://doi.org/10.5194/gmd-9-2973-2016)
744 2016, 2016.

745 Lawrence, D. M., Fisher, R. A., Koven, C. D., Oleson, K. W., Swenson, S. C., Bonan, G., Collier,
746 N., Ghimire, B., van Kampenhout, L., Kennedy, D., Kluzek, E., Lawrence, P. J., Li, F., Li, H.,
747 Lombardozzi, D., Riley, W. J., Sacks, W. J., Shi, M., Vertenstein, M., Wieder, W. R., Xu, C., Ali,
748 A. A., Badger, A. M., Bisht, G., Brunke, M. A., Burns, S. P., Buzan, J., Clark, M., Craig, A.,
749 Dahlin, K., Drewniak, B., Fisher, J. B., Flanner, M., Fox, A. M., Gentine, P., Hoffman, F., Keppel-
750 Aleks, G., Knox, R., Kumar, S., Lenaerts, J., Leung, L. R., Lipscomb, W. H., Lu, Y., Pandey, A.,
751 Pelletier, J. D., Perket, J., Randerson, J. T., Ricciuto, D. M., Sanderson, B. M., Slater, A., Subin,
752 Z. M., Tang, J., Thomas, R. Q., Val Martin, M., and Zeng, X.: The Community Land Model version
753 5: Description of new features, benchmarking, and impact of forcing uncertainty. *Journal of*
754 *Advances in Modeling Earth Systems*, 11(12), 4245–4287, 2019.

755 Le Goff H, Flannigan MD, Bergeron Y. Potential changes in monthly fire risk in the eastern
756 Canadian boreal forest under future climate change. *Canadian journal of forest research*. 2009
757 Dec;39(12):2369-80.

758 Lee, et al. (2020): Expanding the design space of stratospheric aerosol geoengineering to include
759 precipitation-based metrics and explore trade-offs, *Earth System Dynamics*, doi:10.5194/esd-11-
760 1051-2020.

761 Li, F., Zeng, X. D., and Levis, S.: A process-based fire parameterization of intermediate
762 complexity in a Dynamic Global Vegetation Model, *Biogeosciences*, 9, 2761–2780,
763 <https://doi.org/10.5194/bg-9-2761-2012>, 2012.

764 Li, F., Levis, S., and Ward, D. S.: Quantifying the role of fire in the Earth system – Part 1: Improved
765 global fire modeling in the Community Earth System Model (CESM1), *Biogeosciences*, 10, 2293–
766 2314, <https://doi.org/10.5194/bg-10-2293-2013>, 2013.

767 Li, F. and Lawrence, D. M.: Role of fire in the global land water budget during the 20th century
768 through changing ecosystems, *J. Climate*, 30, 1893–908, 2017.

769 Li, F., Lawrence, D. M., and Bond-Lamberty, B.: Impact of fire on global land surface air
770 temperature and energy budget for the 20th century due to changes within ecosystems, *Environ.*
771 *Res. Lett.*, 12, <https://doi.org/10.1088/1748-9326/aa6685>, 2017.

772 Li, F., Lawrence, D. M., and Bond-Lamberty, B.: Human impacts on 20th century fire dynamics
773 and implications for global carbon and water trajectories, *Global Planet. Change*, 162, 18–27, 2018.

774 Li, F., Val Martin, M., Andreae, M. O., Arneth, A., Hantson, S., Kaiser, J. W., Lasslop, G., Yue,
775 C., Bachelet, D., Forrest, M., Kluzek, E., Liu, X., Mangeon, S., Melton, J. R., Ward, D. S.,
776 Darmenov, A., Hickler, T., Ichoku, C., Magi, B. I., Sitch, S., van der Werf, G. R., Wiedinmyer, C.,
777 and Rabin, S. S.: Historical (1700–2012) global multi-model estimates of the fire emissions from
778 the Fire Modeling Intercomparison Project (FireMIP), *Atmos. Chem. Phys.*, 19, 12545–12567,
779 <https://doi.org/10.5194/acp-19-12545-2019>, 2019.

780 Li, Y., Mickley, L. J., Liu, P., and Kaplan, J. O.: Trends and spatial shifts in lightning fires and
781 smoke concentrations in response to 21st century climate over the national forests and parks of the
782 western United States, *Atmos. Chem. Phys.*, 20, 8827–8838, [https://doi.org/10.5194/acp-20-8827-](https://doi.org/10.5194/acp-20-8827-2020)
783 2020, 2020.

784 Li F., D. Lawrence, Y.-Q. Jiang, X.-H. Liu, and Z.-D. Lin, 2022: Fire aerosols slow down the
785 global water cycle, *J. Climate*, [https://journals.ametsoc.org/view/journals/clim/aop/JCLI-D-21-](https://journals.ametsoc.org/view/journals/clim/aop/JCLI-D-21-0817.1/JCLI-D-21-0817.1.xml)
786 0817.1/JCLI-D-21-0817.1.xml.

787 Liu, Y. Q., Stanturf, J., and Goodrick, S.: Trends in global wildfire potential in a changing climate,
788 *Forest Ecol. Manag.*, 259, 685–697, <https://doi.org/10.1016/j.foreco.2009.09.002>, 2010.

789 Liu, Z., Ballantyne, A. P., & Cooper, L. A. (2019). Biophysical feedback of global forest fires on
790 surface temperature. *Nature communications*, 10(1), 1-9.

791 Loehman, R. A. (2020). Drivers of wildfire carbon emissions. *Nature Climate Change*, 1-2.

792 Luo, L. F., Tang, Y., Zhong, S. Y., Bian, X. D., and Heilman, W. E.: Will Future Climate Favor
793 More Erratic Wildfires in the Western United States?, *J. Appl. Meteorol. Climatol.*, 52, 2410–2417,
794 <https://doi.org/10.1175/jamc-d-12-0317.1>, 2013.

795 Meehl, G. A., Arblaster, J. M., Bates, S., Richter, J. H., Tebaldi, C., Gettelman, A., et al.
796 (2020). Characteristics of future warmer basestates in CESM2. *Earth and Space Science*, 7,
797 e2020EA001296. <https://doi.org/10.1029/2020EA001296>.

798 Riahi, K., van Vuuren, D. P., Kriegler, E., Edmonds, J., O'Neill, B. C., Fujimori, S., Bauer, N.,
799 Calvin, K., Dellink, R., Fricko, O., Lutz, W., Popp, A., Cuaresma, J. C., KC, S., Leimbach, M.,
800 Jiang, L., Kram, T., Rao, S., Emmerling, J., Ebi, K., Hasegawa, T., Havlik, P., Humpenöder, F.,
801 Da Silva, L. A., Smith, S., Stehfest, E., Bosetti, V., Eom, J., Gernaat, D., Masui, T., Rogelj, J.,
802 Strefler, J., Drouet, L., Krey, V., Luderer, G., Harmsen, M., Takahashi, K., Baumstark, L.,
803 Doelman, J. C., Kainuma, M., Klimont, Z., Marangoni, G., Lotze-Campen, H., Obersteiner, M.,
804 Tabeau, A., and Tavoni, M.: The Shared Socioeconomic Path ways and their energy, land use, and
805 greenhouse gas emissions implications: An overview, *Global Environ. Chang.*, 42, 153– 168,
806 <https://doi.org/10.1016/j.gloenvcha.2016.05.009>, 2017.

807 Richter, J. H., Tilmes, S., Mills, M. J., Tribbia, J. J., Kravitz, B., Macmartin, D. G., Vitt, F., and
808 Lamarque, J. F.: Stratospheric dynamical response and ozone feedbacks in the presence of SO₂

809 injections, *J. Geophys. Res.-Atmos.*, 122, 12557–12573, <https://doi.org/10.1002/2017JD026912>,
810 2017.

811 O'Neill, B. C., Tebaldi, C., van Vuuren, D. P., Eyring, V., Friedlingstein, P., Hurtt, G., Knutti, R.,
812 Kriegler, E., Lamarque, J.-F., Lowe, J., Meehl, G. A., Moss, R., Riahi, K., and Sanderson, B. M.:
813 The Scenario Model Intercomparison Project (ScenarioMIP) for CMIP6, *Geosci. Model Dev.*, 9,
814 3461–3482, <https://doi.org/10.5194/gmd-9-3461-2016>, 2016.

815 O'Neill BC, Kriegler E, Ebi KL, Kemp-Benedict E, Riahi K, Rothman DS, van Ruijven BJ, van
816 Vuuren DP, Birkmann J, Kok K, Levy M. The roads ahead: Narratives for shared socioeconomic
817 pathways describing world futures in the 21st century. *Global environmental change*. 2017 Jan
818 1;42:169-80.

819 Pechony, O. and Shindell, D.: Driving forces of global wildfires over the past millennium and the
820 forthcoming century, *P. Natl. Acad. Sci. USA*, 107, 19167–19170, doi:10.1073/pnas.1003669107,
821 2010.

822 Pitman AJ, Narisma GT, McAneney J. The impact of climate change on the risk of forest and
823 grassland fires in Australia. *Climatic Change*. 2007 Oct 1;84(3-4):383-401.

824 Randerson, J.T., G.R. van der Werf, L. Giglio, G.J. Collatz, and P.S. Kasibhatla. 2018. Global Fire
825 Emissions Database, Version 4.1 (GFEDv4). ORNL DAAC, Oak Ridge, Tennessee, USA.
826 <https://doi.org/10.3334/ORNLDAAC/1293>.

827 Rey, D. M., Walvoord, M. A., Minsley, B. J., Ebel, B. A., Voss, C. I., & Singha, K. (2020).
828 Wildfire-Initiated Talik development exceeds current thaw projections: Observations and models
829 from Alaska's continuous permafrost zone. *Geophysical Research Letters*, 47,
830 e2020GL087565. <https://doi.org/10.1029/2020GL087565>.

831 Shiogama, H., Hirata, R., Hasegawa, T., Fujimori, S., Ishizaki, N. N., Chatani, S., Watanabe, M.,
832 Mitchell, D., and Lo, Y. T. E.: Historical and future anthropogenic warming effects on droughts,
833 fires and fire emissions of CO₂ and PM_{2.5} in equatorial Asia when 2015-like El Niño events occur,
834 *Earth Syst. Dynam.*, 11, 435–445, <https://doi.org/10.5194/esd-11-435-2020>, 2020.

835 Simpson, I., Tilmes, S., Richter, J., Kravitz, B., MacMartin, D., Mills, M., Fasullo, J., and
836 Pendergrass, A.: The regional hydroclimate response to stratospheric sulfate geoengineering and
837 the role of stratospheric heating, *J. Geophys. Res.-Atmos.*, 124, 2019JD031093,
838 <https://doi.org/10.1029/2019JD031093>, 2019.

839 Stralberg D, Wang X, Parisien MA, Robinne FN, Sólymos P, Mahon CL, Nielsen SE, Bayne EM.
840 Wildfire-mediated vegetation change in boreal forests of Alberta, Canada. *Ecosphere*. 2018
841 Mar;9(3):e02156.

842 Tang et al., Effects of fire diurnal variation and plume rise on U.S. air quality during FIREX-AQ
843 and WE-CAN based on the Multi-Scale Infrastructure for Chemistry and Aerosols (MUSICAv0),
844 *JGR-Atmosphere*, 2022, <https://doi.org/10.1029/2022JD036650>.

845 Tilmes, S., Garcia, R. R., Kinnison, D. E., Gettelman, A., and Rasch, P. J.: Impact of
846 geoengineered aerosols on the troposphere and stratosphere, *J. Geophys. Res.*, 114, D12305,
847 <https://doi.org/10.1029/2008JD011420>, 2009.

848 Tilmes S, Fasullo J, Lamarque JF, Marsh DR, Mills M, Alterskjær K, Muri H, Kristjánsson JE,
849 Boucher O, Schulz M, Cole JN. The hydrological impact of geoengineering in the Geoengineering
850 Model Intercomparison Project (GeoMIP). *Journal of Geophysical Research: Atmospheres*. 2013
851 Oct 16;118(19):11-036.

852 Tilmes, S., Richter, J. H., Kravitz, B., Macmartin, D. G., Mills, M. J., Simpson, I. R., Glanville, A.
853 S., Fasullo, J. T., Phillips, A. S., Lamarque, J. F., Tribbia, J., Edwards, J., Mickelson, S., and Ghosh,
854 S.: CESM1(WACCM) stratospheric aerosol geoengineering large ensemble project, *B. Am.*
855 *Meteorol. Soc.*, 99, 2361– 2371, <https://doi.org/10.1175/BAMS-D-17-0267.1>, 2018.

856 Tilmes, S., Hodzic, A., Emmons, L. K., Mills, M. J., Gettelman, A., Kinnison, D. E., ... &
857 Campuzano-Jost, P. (2019). Climate forcing and trends of organic aerosols in the Community
858 Earth System Model (CESM2). *Journal of Advances in Modeling Earth Systems*, 11(12), 4323-
859 4351.

860 Tilmes, S., MacMartin, D. G., Lenaerts, J. T. M., van Kampenhout, L., Muntjewerf, L., Xia, L.,
861 Harrison, C. S., Krumhardt, K. M., Mills, M. J., Kravitz, B., and Robock, A.: Reaching 1.5 and
862 2.0 °C global surface temperature targets using stratospheric aerosol geoengineering, *Earth Syst.*
863 *Dynam.*, 11, 579– 601, <https://doi.org/10.5194/esd-11-579-2020>, 2020.

864 Tilmes, S., MacMartin, D. G., Lenaerts, J. T. M., van Kampenhout, L., Muntjewerf, L., Xia, L.,
865 Harrison, C. S., Krumhardt, K. M., Mills, M. J., Kravitz, B., and Robock, A.: Reaching 1.5 and
866 2.0 °C global surface temperature targets using stratospheric aerosol geoengineering, *Earth Syst.*
867 *Dynam.*, 11, 579–601, <https://doi.org/10.5194/esd-11-579-2020>, 2020.

868 Val Martin, M., Heald, C. L., Lamarque, J.-F., Tilmes, S., Emmons, L. K., and Schichtel, B. A.:
869 How emissions, climate, and land use change will impact mid-century air quality over the United
870 States: a focus on effects at national parks, *Atmos. Chem. Phys.*, 15, 2805–2823,
871 <https://doi.org/10.5194/acp-15-2805-2015>, 2015.

872 Veira, A., Lasslop, G., and Kloster, S.: Wildfires in a warmer climate: emission fluxes, emission
873 heights, and black carbon concentrations in 2090–2099, *J. Geophys. Res.-Atmos.*, 121, 3195–
874 3223, 2016.

875 Visioni, D., MacMartin, D. G., Kravitz, B., Lee, W., Simpson, I. R., and Richter, J. H.: Reduced
876 poleward transport due to stratospheric heating under stratospheric aerosols geoengineering,
877 *Geophys. Res. Lett.*, 47, e2020GL089470, <https://doi.org/10.1029/2020GL089470>, 2020.

878 Visioni, D., MacMartin, D. G., Kravitz, B., Boucher, O., Jones, A., Lurton, T., Martine, M., Mills,
879 M. J., Nabat, P., Niemeier, U., Séférian, R., and Tilmes, S.: Identifying the sources of uncertainty
880 in climate model simulations of solar radiation modification with the G6sulfur and G6solar
881 Geoengineering Model Intercomparison Project (GeoMIP) simulations, *Atmos. Chem. Phys.*, 21,
882 10039–10063, <https://doi.org/10.5194/acp-21-10039-2021>, 2021a.

883 Visioni D, MacMartin DG, Kravitz B. Is turning down the sun a good proxy for stratospheric
884 sulfate geoengineering?. *Journal of Geophysical Research: Atmospheres*. Mar
885 16;126(5):e2020JD033952, 2021b.

886 van der Werf, G. R., Randerson, J. T., Giglio, L., Collatz, G. J., Kasibhatla, P. S., and Arellano Jr.,
887 A. F.: Interannual variability in global biomass burning emissions from 1997 to 2004, *Atmos.*
888 *Chem. Phys.*, 6, 3423–3441, <https://doi.org/10.5194/acp-6-3423-2006>, 2006.

889 van der Werf, G. R., Randerson, J. T., Giglio, L., Gobron, N., & Dolman, A. J. (2008). Climate
890 controls on the variability of fires in the tropics and subtropics. *Global Biogeochemical Cycles*,
891 22(3).

892 Walker, X. J., Rogers, B. M., Veraverbeke, S., Johnstone, J. F., Baltzer, J. L., Barrett, K., ... &
893 Goetz, S. (2020). Fuel availability not fire weather controls boreal wildfire severity and carbon
894 emissions. *Nature Climate Change*, 1-7.

895 Wang, X., Studens, K., Parisien, M. A., Taylor, S. W., Candau, J. N., Boulanger, Y., & Flannigan,
896 M. D. (2020). Projected changes in fire size from daily spread potential in Canada over the 21st
897 century. *Environmental Research Letters*, 15(10), 104048.

898 Ward, D. S., Kloster, S., Mahowald, N. M., Rogers, B. M., Randerson, J. T., and Hess, P. G.: The
899 changing radiative forcing of fires: global model estimates for past, present and future, *Atmos.*
900 *Chem. Phys.*, 12, 10857–10886, <https://doi.org/10.5194/acp-12-10857-2012>, 2012.

901 Wiedinmyer, C., Quayle, B., Geron, C., Belote, A., McKenzie, D., Zhang, X., O'Neill, S., and
902 Wynne, K. K.: Estimating emissions from fires in North America for air quality modeling, *Atmos.*
903 *Environ.*, 40, 3419–3432, doi:10.1016/j.atmosenv.2006.02.010, 2006.

904 Xia, L., Robock, A., Tilmes, S., and Neely III, R. R.: Stratospheric sulfate geoengineering could
905 enhance the terrestrial photosynthesis rate, *Atmos. Chem. Phys.*, 16, 1479–1489,
906 <https://doi.org/10.5194/acp-16-1479-2016>, 2016.

907 Xia, L., Nowack, P. J., Tilmes, S., and Robock, A.: Impacts of stratospheric sulfate geoengineering
908 on tropospheric ozone, *Atmos. Chem. Phys.*, 17, 11913–11928, [https://doi.org/10.5194/acp-17-](https://doi.org/10.5194/acp-17-11913-2017)
909 11913-2017, 2017.

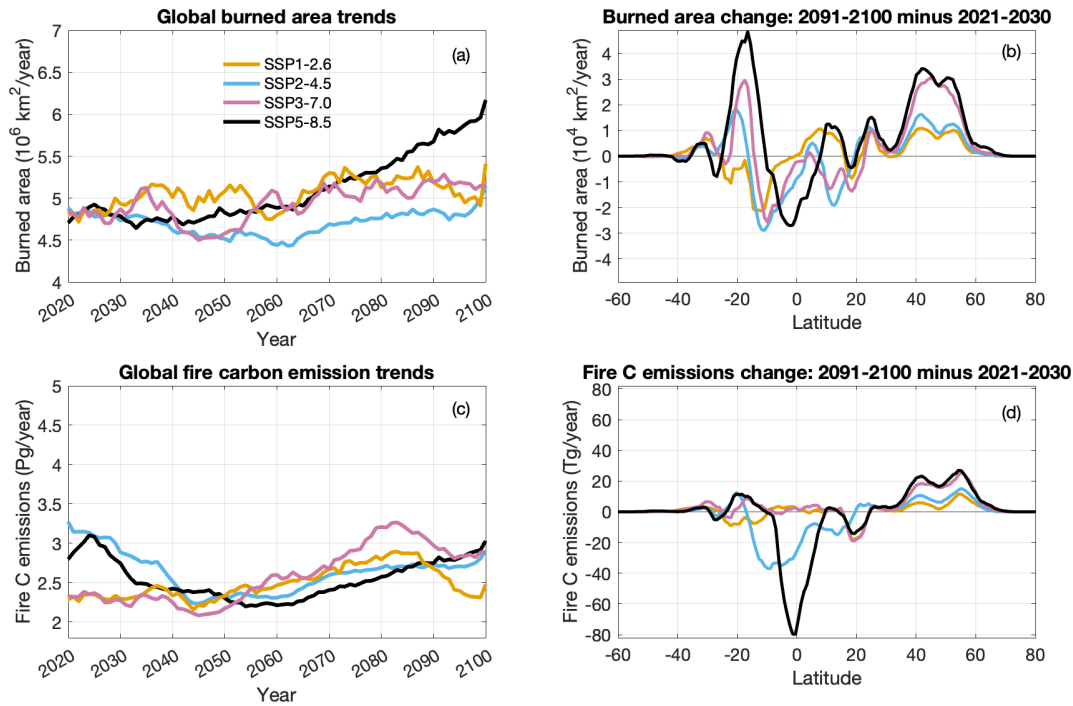
910 Xu, Y., Lin, L., Tilmes, S., Dagon, K., Xia, L., Diao, C., Cheng, W., Wang, Z., Simpson, I., and
911 Burnell, L.: Climate engineering to mitigate the projected 21st-century terrestrial drying of the
912 Americas: a direct comparison of carbon capture and sulfur injection, *Earth Syst. Dynam.*, 11,
913 673–695, <https://doi.org/10.5194/esd-11-673-2020>, 2020.

914 Yue, C., Hantson, S., Ciais, P., & Laurent, P. (2016). Evaluating FireMIP models over boreal
915 regions. *in the FireMIP 2016 Workshop*.

916 Zhang, L., W. Lau, W. Tao, and Z. Li. "Large Wildfires in the Western United States Exacerbated
917 by Tropospheric Drying Linked to a Multi-Decadal Trend in the Expansion of the Hadley
918 Circulation." *Geophysical Research Letters* 47, no. 16 (2020): e2020GL087911.

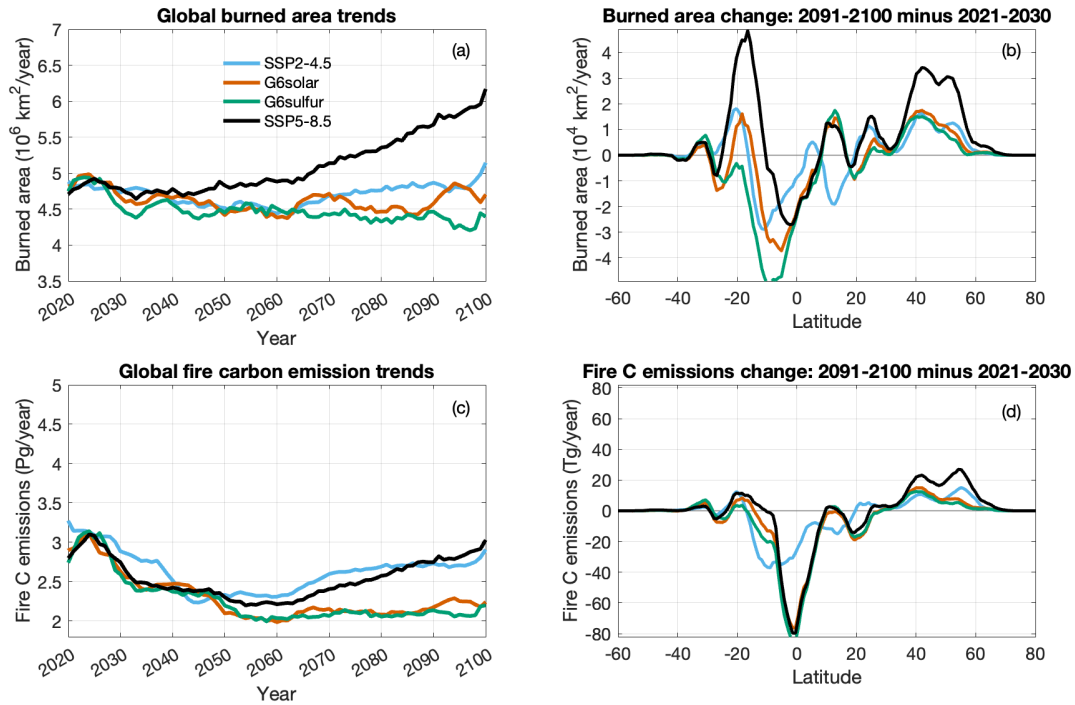
919 Zhang, Y., Fan, J., Shrivastava, M., Homeyer, C.R., Wang, Y. and Seinfeld, J.H., 2022. Notable
920 impact of wildfires in the western United States on weather hazards in the central United States.
921 *Proceedings of the National Academy of Sciences*, 119(44), p.e2207329119.

922
923
924

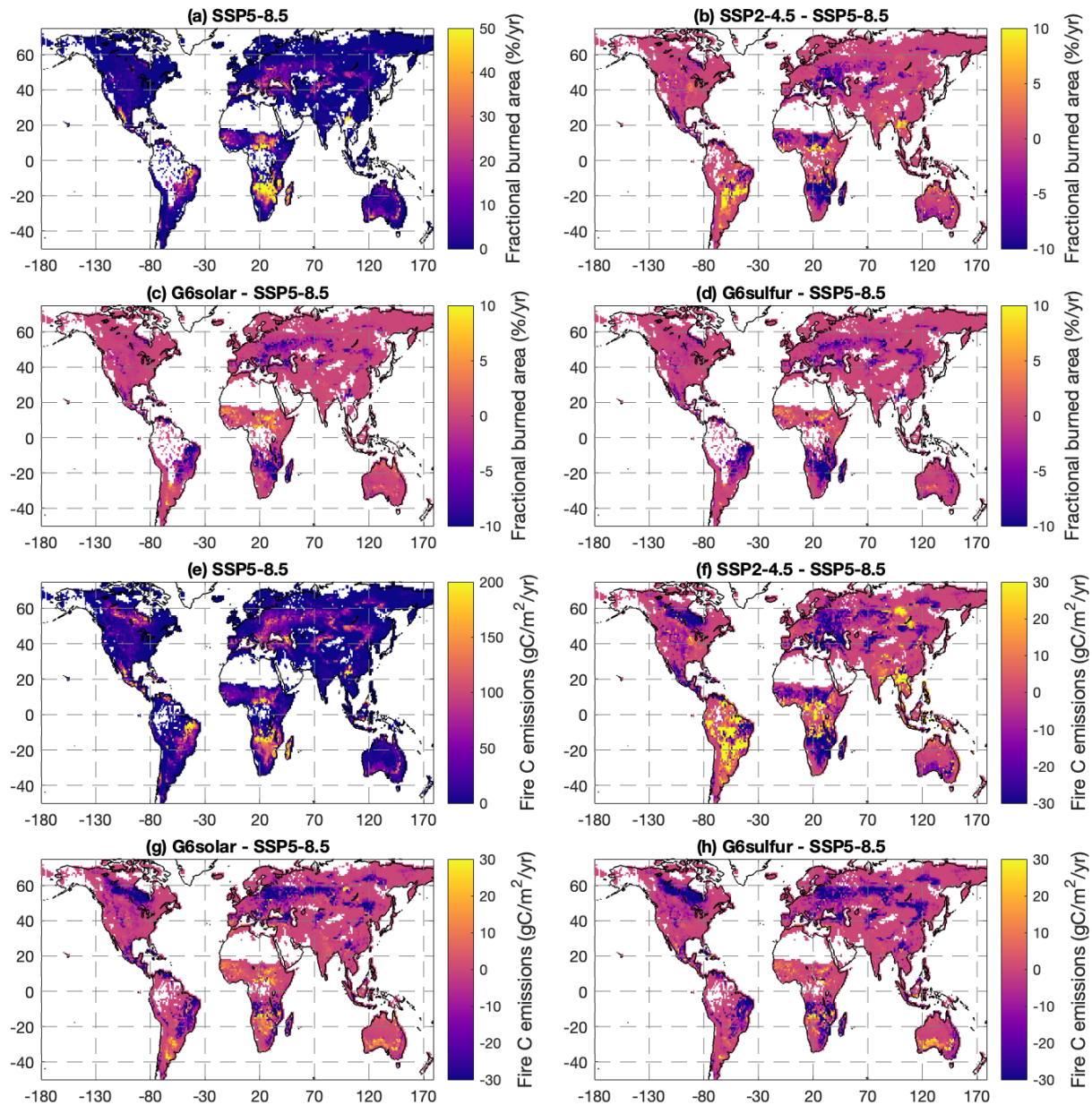


925
 926
 927
 928
 929
 930
 931
 932
 933
 934
 935
 936
 937

Figure 1. Overall global burned area and fire carbon emission trends and changes under SSP scenarios. (a) Time series of global burned area from 2020 to 2100 under the SSP1-2.6, SSP2-4.5, SSP3-7.0, and SSP5-8.5 scenarios (represented by different colors). The time series are shown as 5-year moving averages. (b) Zonal changes (absolute value) of burned area in the period 2091-2100 relative to the period 2021-2030 (calculated by the value in 2091-2100 minus the value in 2021-2030), under the SSP1-2.6, SSP2-4.5, SSP3-7.0, and SSP5-8.5 scenarios (represented by different colors, color code is the same as it in panel a). 5-degree moving average were applied to the shown zonal changes. Panels (c) and (d) are similar to panels (a) and (b), respectively, but for fire carbon emissions.



940
941 **Figure 2.** Overall global burned area and fire carbon emission trends and changes under the
942 G6sulfur and G6solar geoengineering scenarios relative to SSP2-4.5 and SSP5-8.5. (a) Time series
943 of global burned area from 2020 to 2100 under the G6sulfur, G6solar, SSP2-4.5, and SSP5-8.5
944 scenarios (represented by different colors). The time series are shown as 5-year moving averages.
945 (b) Zonal changes (absolute value) of burned area in the period 2091-2100 relative to the period
946 2021-2030 (calculated by the value in 2091-2100 minus the value in 2021-2030), under the
947 G6sulfur, G6solar, SSP2-4.5, and SSP5-8.5 scenarios (represented by different colors, color code
948 is the same as it in panel a). 5-degree moving average were applied to the shown zonal changes.
949 Panels (c) and (d) are similar to panels (a) and (b), respectively, but for fire carbon emissions.
950
951
952

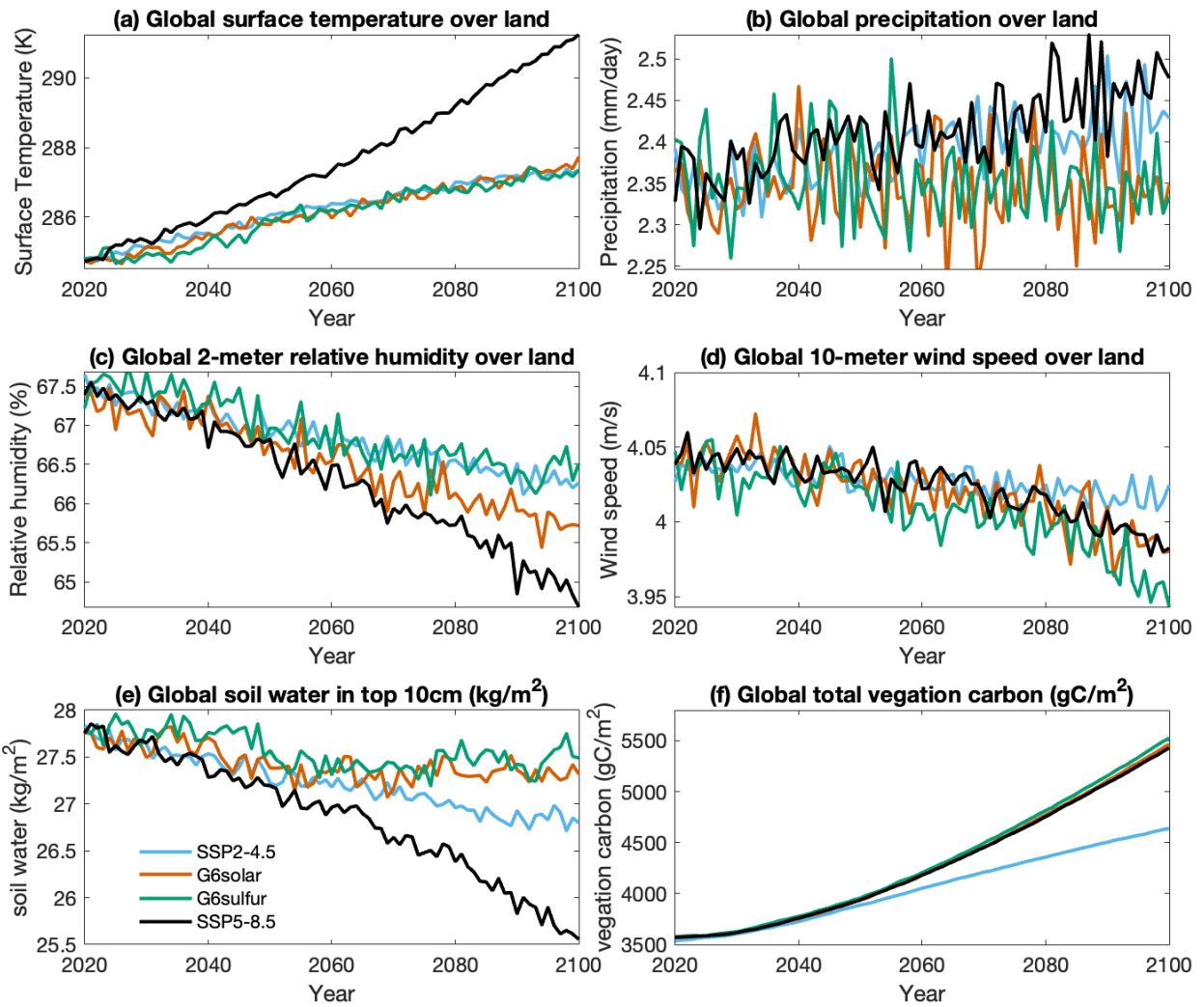


954
955

956 **Figure 3.** Fractional burned area (%/year) and fire carbon missions ($\text{gC}/\text{m}^2/\text{year}$) averaged for
 957 2091-2100. (a) Spatial distribution of fractional burned area (%/year) averaged for 2091-2100
 958 under SSP5-8.5. Results are not shown for model grids where fractional burned area equals to 0.
 959 The difference in fractional burned area of (b) SSP2-4.5 from SSP5-8.5 (c) G6Solar from SSP5-
 960 8.5, and (d) G6Sulfur from SSP5-8.5 averaged for 2091-2100. Results are not shown for model
 961 grids where the difference in fractional burned area equals to 0. (e-h) are similar to (a-d) but for
 962 fire carbon missions ($\text{gC}/\text{m}^2/\text{year}$). For a scenario with multiple simulations (i.e., SSP5-8.5, SSP2-
 963 4.5, G6Sulfur, and G6Solar), simulation mean is shown.

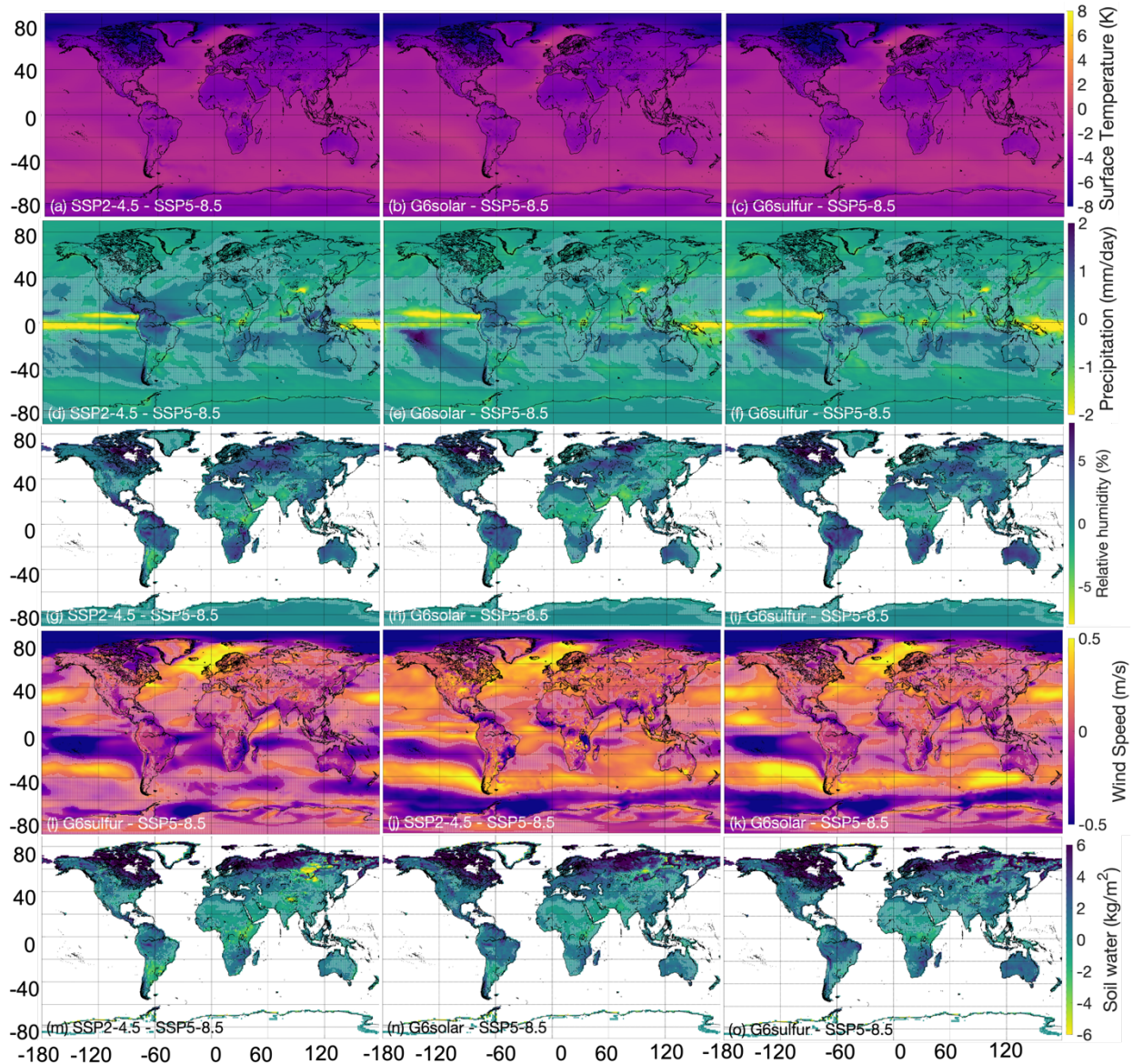
964
965

966
967
968



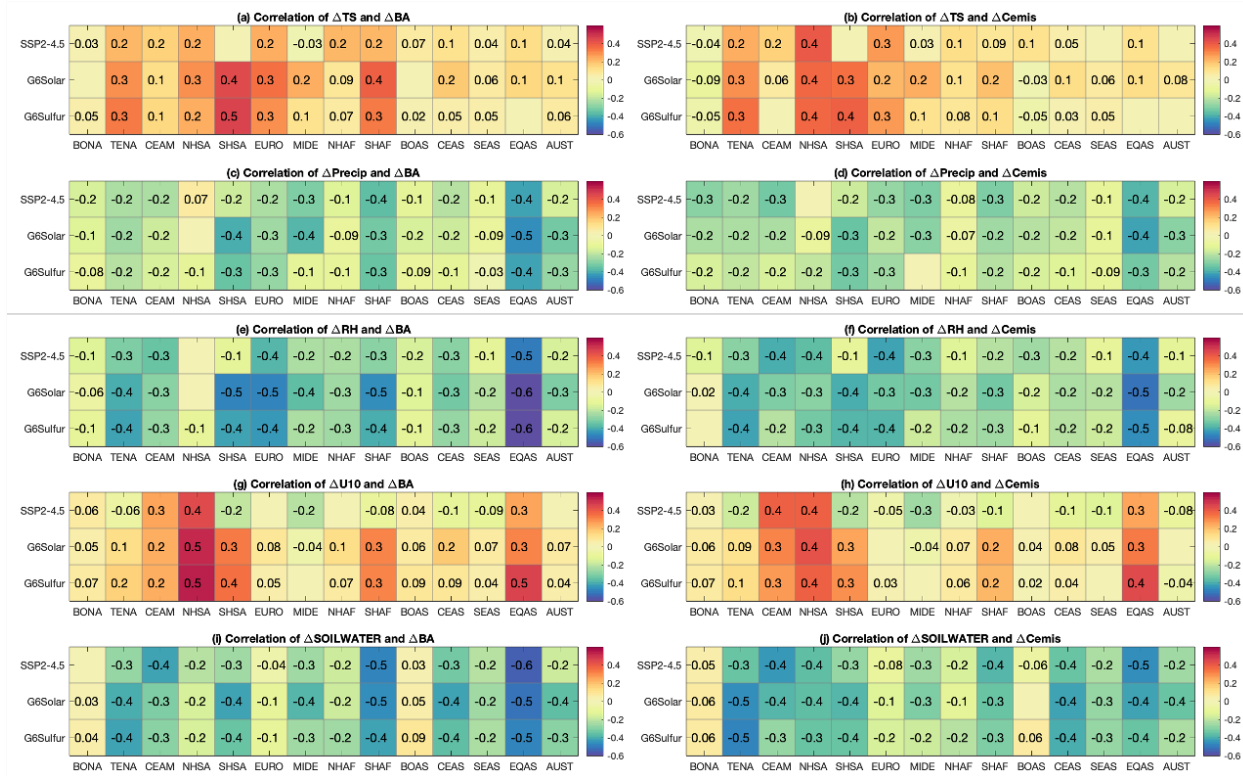
969
970
971
972
973
974
975
976
977

Figure 4. Time series of mean (a) surface temperature (K), (b) precipitation (mm/day) over the land, (c) 2-meter relative humidity (%) over the land, (d) 10-meter wind speed (m/s) over the land, (e) soil water content at top 10 cm (kg/m^2), and (f) vegetation carbon excluding carbon pool (Gc/m^2). For a scenario with multiple simulations (i.e., SSP5-8.5, SSP2-4.5, G6Sulfur, and G6Solar), simulation means are shown.



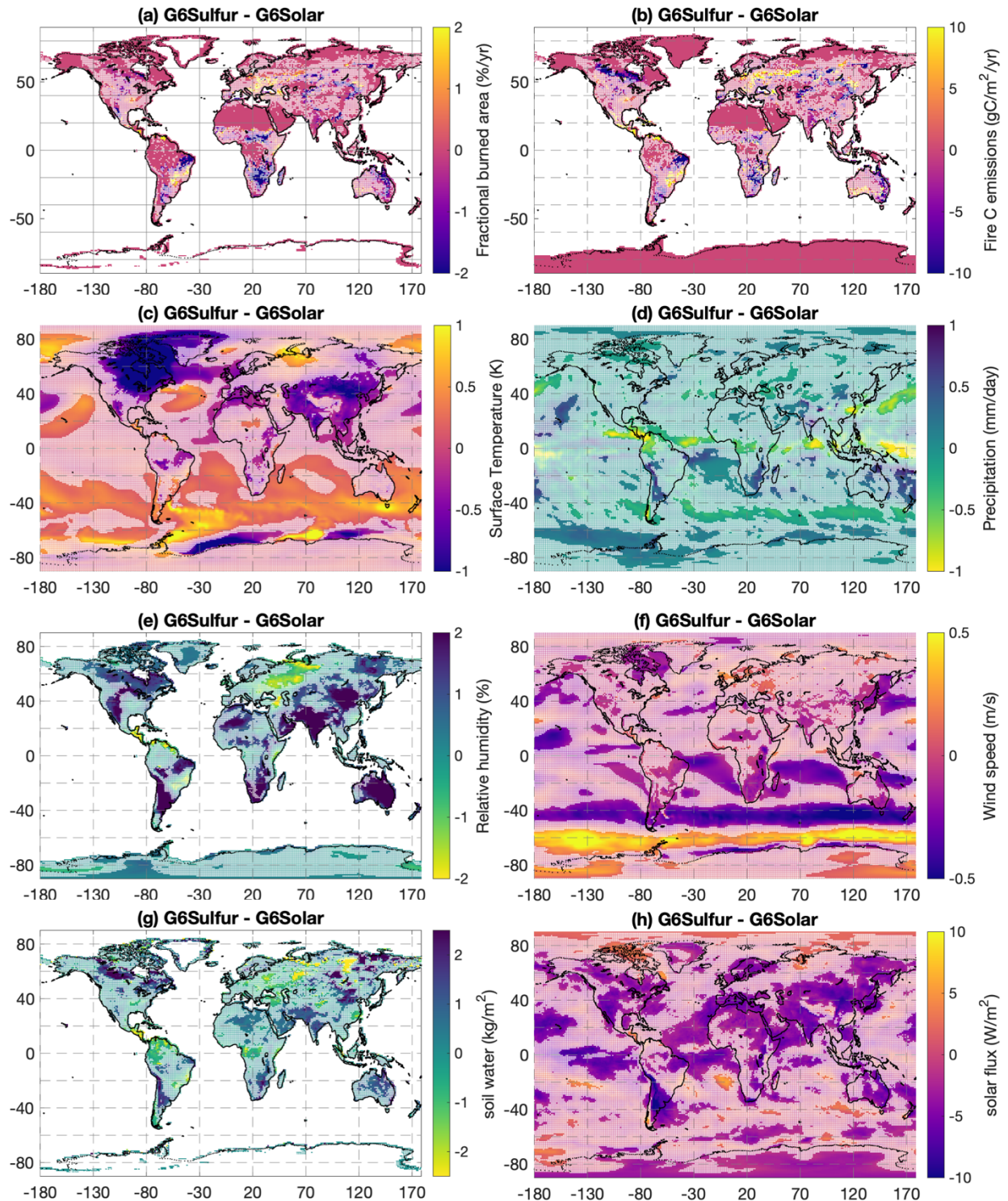
978
 979
 980
 981
 982
 983
 984
 985
 986
 987
 988
 989
 990

Figure 5. The difference in surface temperature (K) of (a) SSP2-4.5 from SSP5-8.5 (b) G6Solar from SSP5-8.5, (c) G6Sulfur from SSP5-8.5 averaged for 2091-2100. (d-f) are the same as (a-c) but for precipitation (mm/day). (g-i) are the same as (a-c) but for 2-meter relative humidity (%). (j-l) are the same as (a-c) but for 10-meter wind speed (m/s). (m-o) are the same as (a-c) but for soil water content at top 10 cm (kg/m^2). The grids where SSP2-4.5, G6Sulfur, or G6Solar is not significantly different from SSP5-8.5 is marked with white shade. Taking precipitation of SSP2-4.5 as an example, the significance for each model grid is calculated by student t-test (p value is 0.1) using 10 years of SSP2-4.5 precipitation data during 2091-2100 (10 data points) and 10 years of SSP5-8.5 precipitation data during 2091-2100 (10 data points).



992
 993
 994
 995
 996
 997
 998
 999
 1000
 1001
 1002
 1003
 1004
 1005
 1006
 1007
 1008
 1009
 1010
 1011
 1012
 1013
 1014

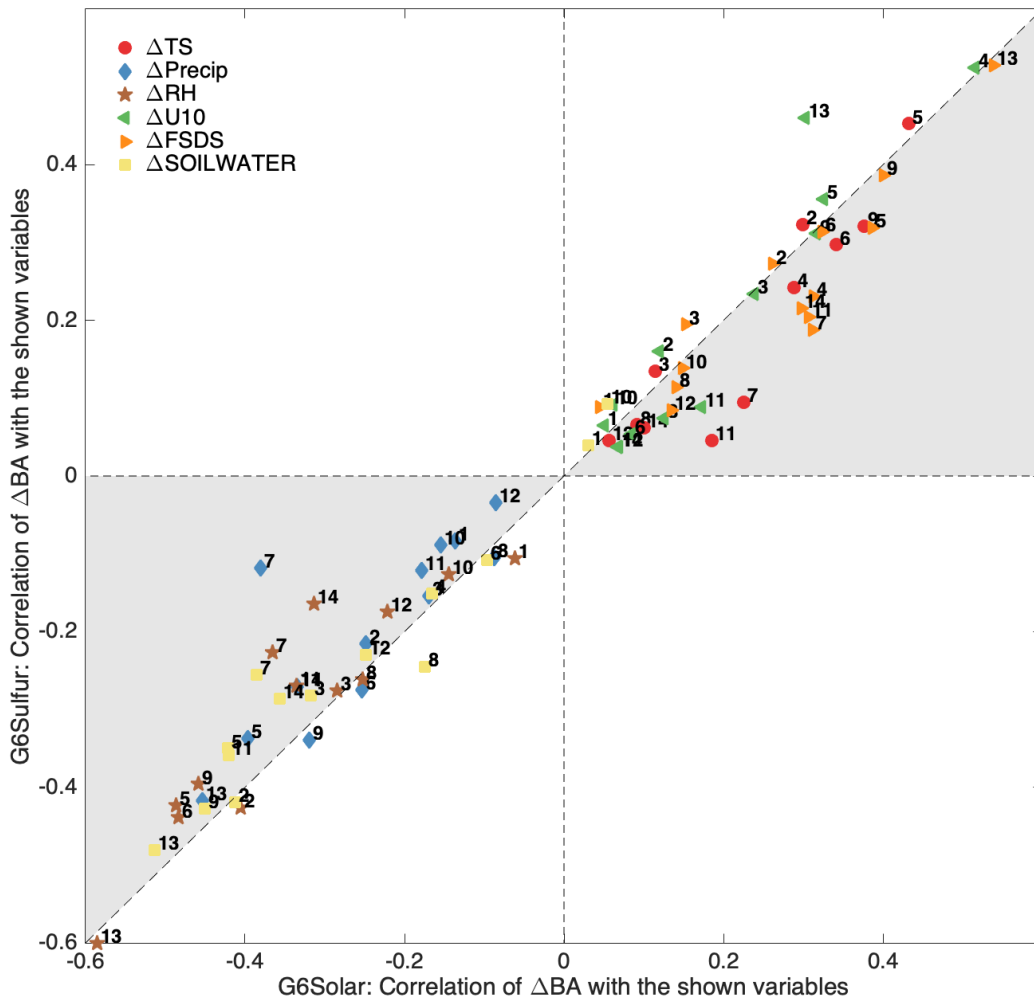
Figure 6. Correlations of (a) surface temperature change (ΔTS) and burned area change for SSP2-4.5, G6Solar, and G6Sulfur, and (b) ΔTS and fire carbon emission change ($\Delta Cemis$) for SSP2-4.5, G6Solar, and G6Sulfur. Only correlations that are significant are labeled (p value ≤ 0.1). For SSP2-4.5, ΔTS is calculated for individual model grids within the region and annual values. It is defined as TS of SSP2-4.5 minus TS of SSP5-8.5 (the reference case). For G6Solar and G6Sulfur, ΔTS is defined in the same way as SSP2-4.5. ΔBA and $\Delta Cemis$ are defined in the same way as ΔTS . (c-d) are the same as (a-b) but for precipitation change ($\Delta Precip$). (e-f) are the same as (a-b) but for relative humidity change (ΔRH). (g-h) are the same as (a-b) but for 10-meter wind speed change ($\Delta U10$). (i-j) are the same as (a-b) but for the change in soil water content at top 10 cm ($\Delta SOILWATER$). Correlations are calculated for 14 fire regions (x-axis), following Giglio et al. (2010), namely Boreal North America (BONA), Temperate North America (TENA), Central America (CEAM), Northern Hemisphere South America (NHSA), Southern Hemisphere South America (SHSA), Europe (EURO), Middle East (MIDE), Northern Hemisphere Africa (NHAF), Southern Hemisphere Africa (SHAF), Boreal Asia (BOAS), Central Asia (CEAS), Southeast Asia (SEAS), Equatorial Asia (EQAS), and Australia and New Zealand (AUST). The definition of the regions can be found in Figure S3.



1015
 1016 **Figure 7.** The difference between G6Sulfur and G6Solar in (a) burned area fraction (BA; %/yr),
 1017 (b) fire carbon emissions (Cemis; gC/m²/yr), (c) surface temperature (TS; K), (d) precipitation
 1018 (Precip; mm/day), (e) 2-meter relative humidity (RH; %), (f) 10-meter wind speed (U10; m/s), (g)
 1019 soil water content at top 10 cm (Soilwater; kg/m²), and (h) downwelling solar flux at the surface
 1020 (FSDS; W/m²) averaged for 2091-2100. The grids where SSP2-4.5, G6Sulfur, or G6Solar is not
 1021 significantly different from SSP5-8.5 is marked with white shade. Taking precipitation of SSP2-

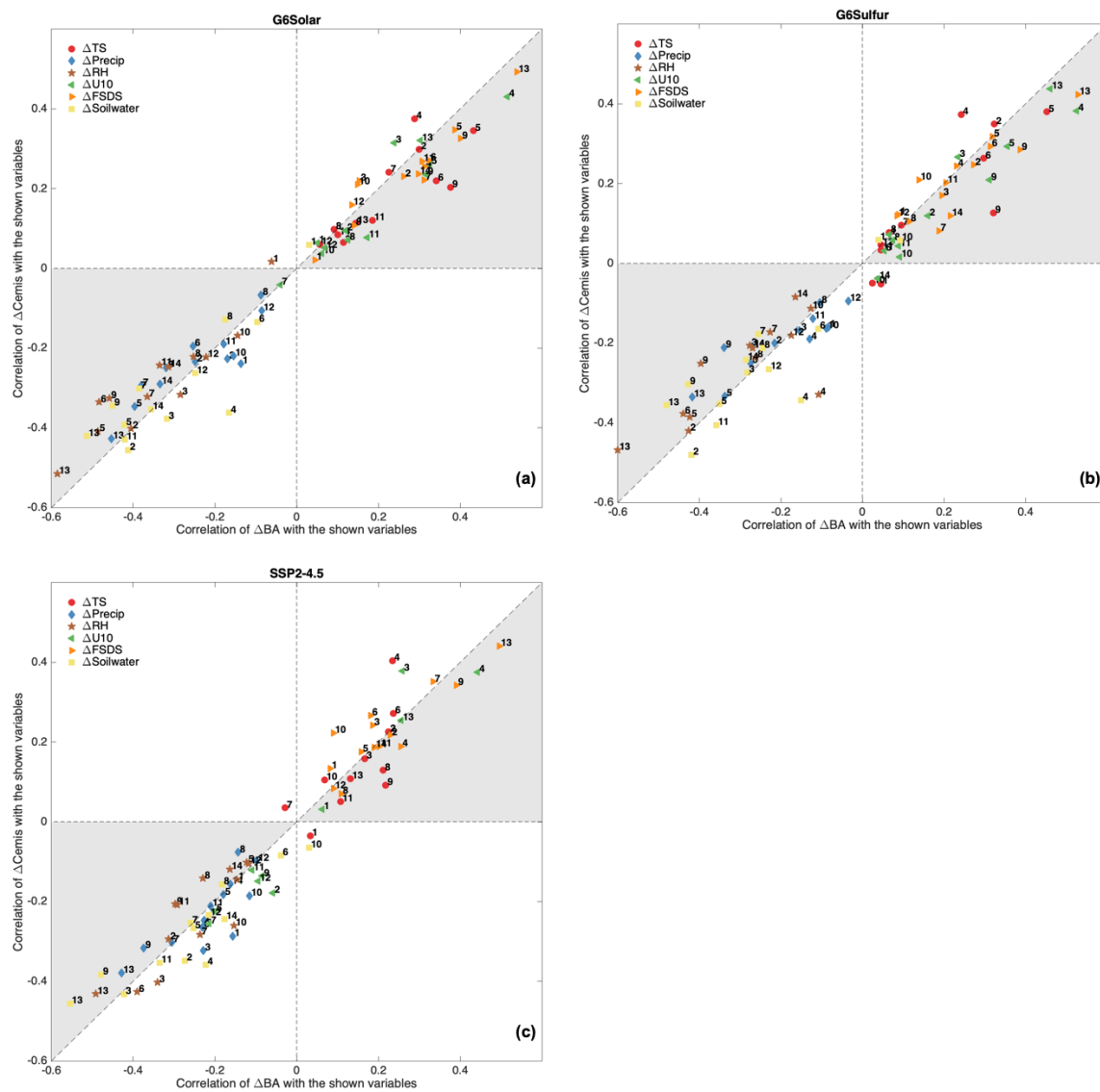
1022 4.5 as an example, the significance for each model grid is calculated by student t-test (p value is
 1023 0.1) using 10 years of SSP2-4.5 precipitation data during 2091-2100 (10 data points) and 10 years
 1024 of SSP5-8.5 precipitation data during 2091-2100 (10 data points).

1025
 1026
 1027
 1028
 1029
 1030



1031
 1032 **Figure 8.** Correlations between burned area change in G6Solar from SSP5-8.5 (ΔBA) with the
 1033 change in other variables in G6Solar from SSP5-8.5 (x-axis) versus correlations between burned

1034 area change in G6Sulfur from SSP5-8.5 (Δ BA) with the change in other variables in G6Sulfur
 1035 from SSP5-8.5 (y-axis). The variables shown here are surface temperature change (Δ TS),
 1036 precipitation change (Δ Precip), 2-meter relative humidity change (Δ RH), 10-meter wind speed
 1037 change (Δ U10), soil water content in top 10 cm change (Δ SOILWATER), and downwelling solar
 1038 flux at the surface change (Δ FSDS). All “changes” refer to 2091-2100 averages. The numbers
 1039 labeled in the figure correspond to the region: 1–Boreal North America, 2–Temperate North
 1040 America, 3–Central America, 4–Northern Hemisphere South America, 5–Southern Hemisphere
 1041 South America, 6–Europe, 7–Middle East, 8–Northern Hemisphere Africa, 9–Southern
 1042 Hemisphere Africa, 10–Boreal Asia, 11–Central Asia, 12–Southeast Asia, 13–Equatorial Asia, and
 1043 14–Australia and New Zealand. The definition of the regions can be found in Figure S3. The shade
 1044 highlights where correlation with Δ BA is larger than correlation with Δ Cemis. See Figure S13 for
 1045 plots with variables separately presented.



1046
 1047 **Figure 9.** (a) Correlations between burned area change in G6Solar from SSP5-8.5 (Δ BA) with the
 1048 change in other variables in G6Solar from SSP5-8.5 (x-axis) versus correlations between fire

1049 carbon emission change in G6Solar from SSP5-8.5 (ΔC_{emis}) with the change in other variables in
1050 G6Solar from SSP5-8.5 (y-axis). The variables shown here are surface temperature change (ΔTS),
1051 precipitation change ($\Delta Precip$), 2-meter relative humidity change (ΔRH), 10-meter wind speed
1052 change (ΔU_{10}), soil water content in top 10 cm change ($\Delta SOILWATER$), and downwelling solar
1053 flux at the surface change ($\Delta FSDS$). All “changes” refer to 2091-2100 averages. The numbers
1054 labeled in the figure correspond to the region: 1–Boreal North America, 2–Temperate North
1055 America, 3–Central America, 4–Northern Hemisphere South America, 5–Southern Hemisphere
1056 South America, 6–Europe, 7–Middle East, 8–Northern Hemisphere Africa, 9–Southern
1057 Hemisphere Africa, 10–Boreal Asia, 11–Central Asia, 12–Southeast Asia, 13–Equatorial Asia, and
1058 14–Australia and New Zealand. The definition of the regions can be found in Figure S3. The shade
1059 highlights where correlation with ΔBA is larger than correlation with ΔC_{emis} . (b) is the same as
1060 (a) but for G6Sulfur. (c) is the same as (a) but for SSP2-4.5. See Figure S14-S16 for plots with
1061 variables separately presented.